Assessing cost-effectiveness of nature-based solutions scenarios: Integrating hydrological impacts and life cycle costs

Yangzi Qiu, Daniel Schertzer, Ioulia Tchiguirinskaia

Version of Record: https://www.sciencedirect.com/science/article/pii/S0959652621039160
Manuscript_4fcf35002529d2dcdea6664396271853

Assessing cost-effectiveness of nature-based solutions scenarios: integrating hydrological impacts and life cycle costs

Yangzi Qiu[1], Daniel Schertzer[1], Ioulia Tchiguirinskaia[1]

[1]Hydrology Meteorology & Complexity, École des Ponts ParisTech, Champs-sur-Marne,77455, France

Correspondence to: Yangzi Qiu (yangzi.qiu@enpc.fr)

Abstract: Nature-based solutions (NBS) as a sustainable strategy has recently received increasing attention for urban stormwater management. Thus, an evaluation of cost-effectiveness of NBS scenarios by integrating hydrological impacts and life cycle costs is significant for the decision-making process. This study first investigates the hydrological responses of a 5.2 km^2 semi-urban watershed under various implementation NBS scenarios and highly spatially variable rainfall fields. The fractal dimension is considered as a scale invariance indicator to quantify the heterogeneous spatial distributions of NBS in each scenario across a range of scales. The hydrological responses of NBS scenarios are assessed by the fully distributed and physically based model (Multi-Hydro) under different rainfall conditions with a high spatial resolution of 10 m. In order to assess the cost-effective NBS scenarios, the hydrologic indicator (reduction of peak flow and total runoff volume) is integrated with the economic indicator (life cycle costs). The results show that the optimal NBS scenarios are characterised with fractal dimension ranges from 1.5 to 1.6 under all studied rainfall events. Considering the NBS scenarios under the strongest rainfall event, concentrating NBS downstream of the catchment can be more cost-effective. This study can provide some guidelines for the decision-making process on sustainable urban planning and improve the flood resilience of cities.

Keywords: Nature-based solutions; Urban stormwater management; Hydrological impacts; Cost-effectiveness; Life cycle costs

1. Introduction

A typical urbanisation process is always accompanied by increasing impervious surfaces, such as an expansion of roads and buildings (Ercolani et al., 2018). To a certain extent, these modifications reduce the rainfall infiltration and increase surface runoff, thereby enlarging the pressure of the urban drainage system, especially for extreme storms, which is possible to cause urban flooding (Grebel et al., 2013). In recent years, nature-based solutions (NBS) is considered a sustainable strategy that has been aroused widespread concern to reduce the occurrence of these natural calamities. European Commission (2015) has defined NBS as the measures inspired and supported by nature, which are cost-effective, and simultaneously provide multiple benefits in terms of environmental, social and economic and promote resilience. In practise, it is commonly considered to implement a series of small-scale green infrastructures (e.g. porous pavements, green roofs, rain gardens, and bioretentions) in urban catchments to drive the modified regimes back to pre-development hydrologic regimes (Eckart et al., 2017). Albert et al. (2017) have defined three criteria for the application of NBS: (i) to offer continuous benefits for society, economy and nature; (ii) to act as a transdisciplinary umbrella that incorporates experience from existing approaches; and (iii) to refine the NBS application in real-life settings.

In the last decade, NBS has presented some contributions to manage the stormwater runoff (Palla and Gnecco, 2015; Ahiablame and Shakya, 2016). For investigating the hydrological impacts of NBS, researchers have gradually shifted their interest from experimental sites at the single scale

(Berretta et al., 2014; Stanić et al., 2019) to the modelling at the urban catchment scale (Cipolla et al., 2016; Versini et al., 2016). For instance, a number of hydrological models are adopted for predicting the hydrological responses of NBS in different urban catchments (Liu et al., 2015; Her et al., 2017). Among these modelling-based studies, most of them applied the semi-distributed Storm Water Management Model (SWMM) (Luan et al., 2019), which can only represent the NBS as the percentage in each sub-catchment (Guo et al., 2019). Recently, some studies have used fully distributed hydrological models to simulate the hydrological impacts of spatial distributions of NBS at the urban catchment scale (Versini et al., 2016; Fry and Maxwell, 2017; Qiu et al., 2021). For instance, Fry and Maxwell (2017) indicated that the spatial location of NBS along principal flow paths is more critical than the amount of NBS implemented within the watershed.

Nevertheless, the researches mentioned above focused only on the infiltration, retention and detention performance of NBS in terms of technical criteria. Indeed, few studies considered both technical and economic criteria to assess the cost-effectiveness of NBS alternatives (Liao et al., 2013; Li et al., 2020). Hua et al. (2020) and Campos et al. (2020) pointed out that the multi-criteria analysis approach was significant for evaluating future NBS scenarios because the importance of each criterion was quite different, and they needed to be integrated into the evaluation process to quantify and find an optimal alternative. For instance, Luan et al. (2019) and Hua et al. (2020) had used the integrated evaluation method to evaluate the performances of different land use scenarios with the implantation of various types of NBS in an urban catchment. Nevertheless, they used the semi-distributed model and design storm, which did not consider the spatial heterogeneity distribution of NBS and small-scale rainfall variability. Thus, the predictions of hydrological responses of NBS scenarios are not entirely reliable and affect the optimisation of cost-effective

alternatives. Furthermore, it is important to note that previous studies used classical metrics, like the percentage, to quantify the implementation degree of NBS in catchments. However, the percentage of area required to implement NBS depends on the resolution of the model, which remains a scale-dependent quantity. Hence, a scale-independent indicator, such as fractal dimension, is more physically relevant to quantify the heterogeneity of spatial distributions of NBS and propagate their implementation level from the smallest scale to the outer scale of the catchment (Versini et al., 2020).

Based on the earlier studies, several main scientific gaps or shortages still exist and will be covered by this study:

(i) The hydrological responses of the NBS scenarios need to be further investigated in terms of small-scale rainfall variability and spatial distributions of NBS. Here, the small-scale rainfall variability is presented by the high-resolution polarimetric X-band radar data of École des Ponts ParisTech (ENPC). The fully distributed and physically-based hydrological model (Multi-Hydro) is used to consider the heterogeneity of NBS distributions with a high spatial resolution of 10 m.

(ii) A series of NBS scenarios are created in different implementation levels, spatial distributions and initial conditions. To quantify the heterogeneity of spatial distributions and implementation levels of NBS across scales, the scale invariance indicator of fractal dimension is used.

(iii) The technical and economic indicators are integrated to assess the cost-effectiveness of the NBS scenarios. The technical indicators are based on the reduction of peak flow and total runoff volume of the NBS scenarios under different space-time rainfall events. The economic indicator corresponds to the life cycle costs (LCC) of each NBS scenario.

2. Materials and Method

Assessing the cost-effectiveness of NBS scenarios in urban catchments needs a watershed strategy informed by understanding potential hydrological mechanisms and economic costs. This study takes the Guyancourt catchment as a pilot site. The study context, the selected rainfall events and the Multi-hydro model are presented in detail in the following subsections.

2.1. Study context

The Guyancourt city (located in the southwestern suburbs of Paris), a 5.2 km^2 semi-urban catchment, is selected for this study (Fig. 1). Because this study area has been detailed in Qiu et al. (2021), only some primary elements are presented here. As shown in Fig. 1, the catchment includes seven main land use types with an imperviousness of around 37 %. For the roads, 47.8 % of them are the non-driveways with width range from 1.5 to 2.5 m, and 52.2 % are the secondary roads (2.5 m < width < 5.5 m) and main road (width > 7 m). For the buildings, 76.3 % of them are public buildings (apartment, industrial, commercial), mainly located in the north of catchment with flat roofs, which are suitable for implementing different types of green roof (i.e. extensive, semi-intensive and intensive). There exist 23.6 % of houses with sloped roofs (≤ 15°), which are only suitable for converting to extensive green roofs. The Digital Elevation Model (DEM) with a resolution of 10 m is obtained by interpolation of the raw DEM data (25 m) from IGN (as shown in Fig. 2a). The whole catchment is relatively flat, with elevation ranges from 143.39 to 175.1 m. The drainage system of the catchment has been managed by the local authority of the agglomeration community of Saint-Quentin-en-Yvelines, which contains 4474 conduits and 4534 nodes (see Fig. 2b). Large parts of the conduits (around 70 %) have the width from 0.2 to 0.5 m, and the main conduits are designed

with the width between 0.9 and 1.6 m to convey the flow in the whole catchment to the outlet.

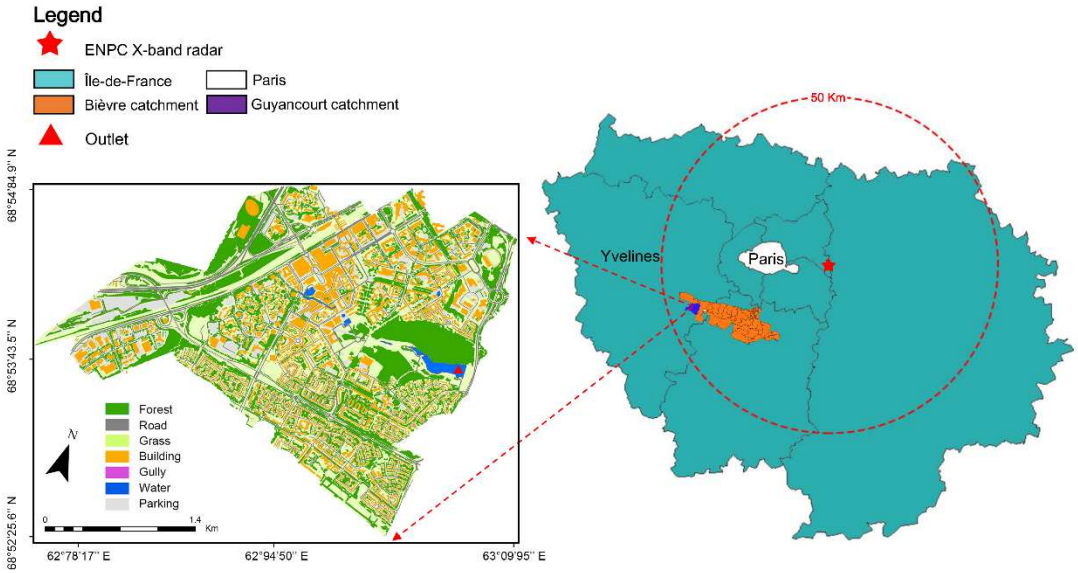

Fig. 1. Location and land use map of Guyancourt catchment.

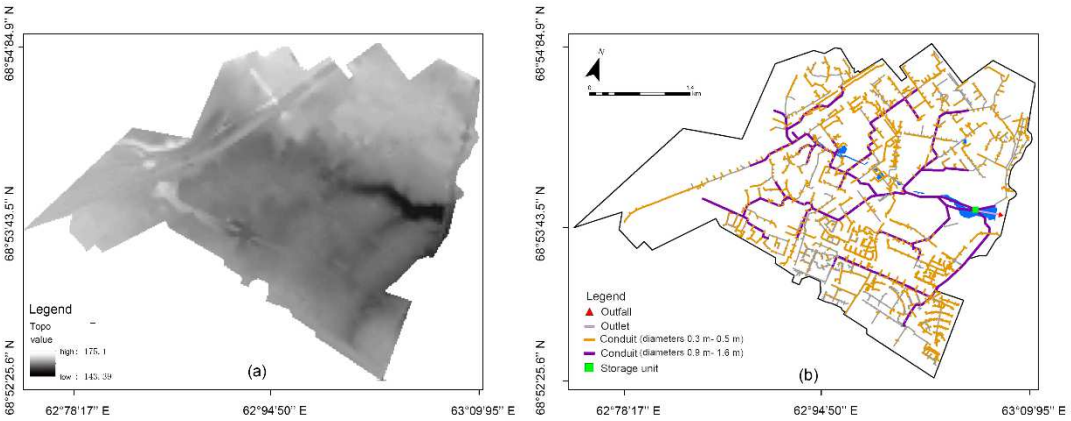

Fig. 2. (a) Elevation of Guyancourt catchment (10 m resolution); (b) the spatial distribution of the conduits in the drainage system.

2.2. Rainfall events

The distributed rainfall data were retrieved from the ENPC polarimetric X-band radar, which is characterised by the spatial and temporal resolution of 250 m and 3.41 min, respectively. In this study, three long rainfall events (12-13/09/2015, 16/09/2015, 05-06/10/2015) with durations of 44 h,

8.5 h and 31 h occurred after a particularly dry period in France in 2015. These rainfall episodes are not very strong but fairly typical for this region, with the cumulative rainfall of 31.5 mm, 12 mm and 20 mm, respectively. They were first selected and then subdivided into eight short rainfall events (EV1-EV8). According to the Montana formula (Gutierrez-Lopez et al., 2019), the return periods of the subdivided rainfall periods range from 0.2 months to 20 years. These common rainfall events can be more representative than extreme ones for assessing NBS performances (Versini et al., 2015). The duration of these subdivided rainfall events was artificially set to 3 hours to limit the high rainfall intermittency. The areal-averaged cumulative rainfall of 48 h before the studied events ranges between 0 and 24.2 mm, and that of the maximum instantaneous intensity are ranges from 0 to 20.6 mm h^{-1} (see Table 1). Here, we performed a sensitivity analysis for the catchment regarding the soil is saturated at the beginning of EV1. The results show that the simulated flow maximum increased by 10.5 % at the second rainfall peak. Future studies will use longer rainfall time series to simulate the catchment responses before the event and investigate the effects of soil moisture conditions. However, to focus on the fast response of the catchment at the rainfall event scale and limit the effects of the multi-event soil moisture conditions on the NBS simulations, we assumed a dry antecedent moisture condition for each simulated event in this study.

The main characteristics of these eight rainfall events differ in their total amounts and intensity (see more details in Table 1). The areal-averaged rainfall intensity (mm h^{-1}) and the cumulative rainfall (mm) of the selected rainfall events are shown in Fig. 3. It is noticed that the two strongest rainfall events are EV2 and EV8, with the areal-averaged peak rainfall intensity corresponding to 20.6 mm h^{-1} and 36.4 mm h^{-1}, respectively. The maximum rainfall intensity of per radar pixel of the two strongest events (Table 1) is 41.2 mm h^{-1} and 55.6 mm h^{-1}, respectively, indicating that some

locations are characterised by strong rainfall cells. The other rainfall events are relatively weak, with the areal-averaged maximum rainfall intensity ranging from 2.91 mm h^{-1} to 9.03 mm h^{-1}. However, the maximum rainfall intensity of per radar pixel of these events ranges from 5.33 mm h^{-1} to 29.1 mm h^{-1}. Apparently, for these rainfall events, the rainfall intensity of per radar pixel has an extensive range of spectrum. Concerning the total amounts (cumulative rainfall) of each event, the EV2 is the highest, with the cumulative rainfall by averaged in space and per radar pixel around 5.46 mm and 8.14 mm, respectively (as shown in Figs. 3 and 4). Although EV8 has a higher peak rainfall intensity than EV2, it only lasts for a few minutes, which is not significant for the cumulative rainfall.

Table 1. The main characteristics of the selected rainfall events.

Event ID	**Date**	**Duration (h)**	**Maximum intensity (mm h^{-1}) (average/per pixel)**	**Cumulative rainfall (mm) (average/maximum per pixel)**	**Maximum intensity (mm h^{-1})/Cumulative rainfall (mm) (48 h before)**
EV1	13/September/2015	3 h	7.68/19.7	2.96/3.89	20.6/18.8
EV2	13/September/2015		20.6/41.2	5.46/8.14	13.0/13.3
EV3	16/September/2015		9.03/29.1	4.66/5.35	4.1/16.1
EV4	16/September/2015		5.55/9.53	2.32/2.58	8.0/24.2
EV5	05/September/2015		3.87/6.9	1.48/1.77	0.0/0.0
EV6	05/October/2015		4.11/6.72	3.86/4.05	5.1/4.5
EV7	05/October /2015		2.91/5.33	2.75/3.43	5.5/7.5
EV8	06/ October /2015		36.4/55.6	4.11/8.01	5.5/11.7

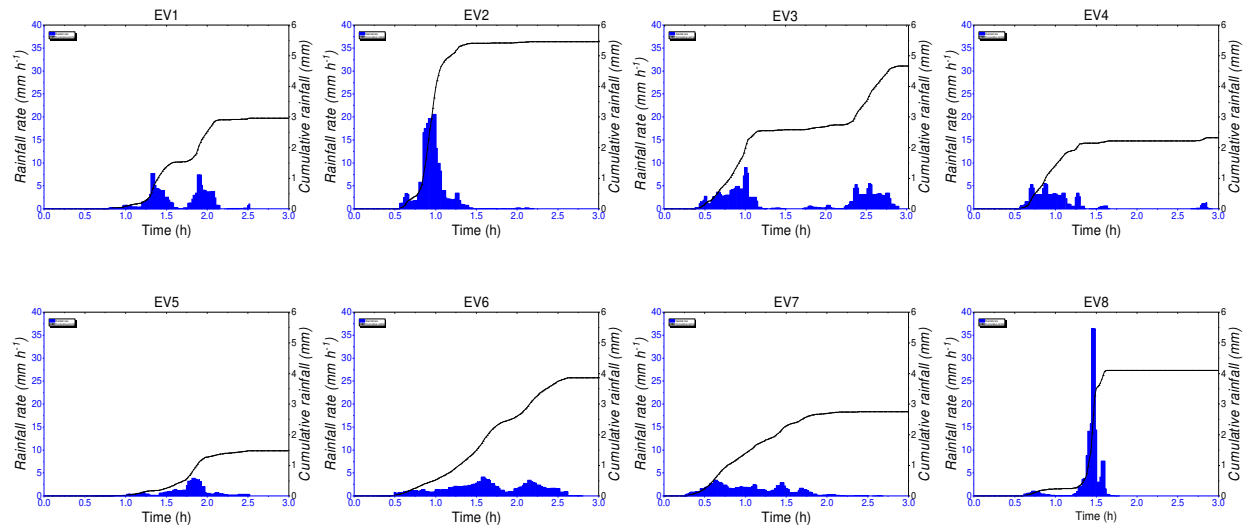

Fig. 3. The areal-averaged rainfall intensity (mm h^{-1}) and cumulative rainfall (mm) over the whole catchment of the selected rainfall events.

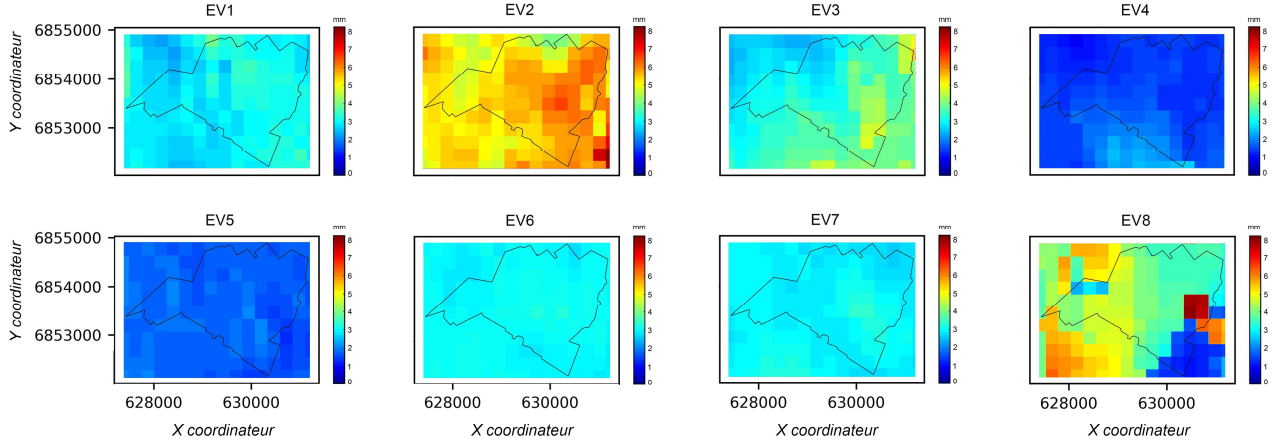

Fig. 4. The cumulative rainfall (per radar pixel) over the whole catchment of the eight selected rainfall events.

2.3. Multi-Hydro model

The Multi-Hydro model is a fully distributed and physically-based hydrological model developed at ENPC (El-Tabach et al. 2009; Giangola-murzyn, 2013; Ichiba 2016). Because the model is identical to those used by Qiu et al. (2021), only the essential elements are summarised here. Multi-Hydro is the coupling core that making the interaction between several widely validated

existing models. Each model represents a part of the urban water cycle (see Ichiba et al., 2018 for a flow-process diagram of the model). Because of the interactive character of Multi-Hydro, the interaction between each model can be chosen by users based on their needs. In this study, only the interactions (inputs or outputs of water) between the surface model and the drainage model are used, and they are carried out with the loop of 3 min. The surface model is based on the TREX model (Velleux et al., 2008), which simulates the surface runoff and infiltration processes concerning the pixels defined for different land uses. The surface runoff is simulated by a diffusive wave approximation of 2D Saint-Venant equations, and superficial infiltration processes are governed by the simplification of the Green and Ampt equation. The drainage model takes the source of the 1D SWMM (Rossman, 2010), which used Saint-Venant equations to calculate the flow in the drainage system. Furthermore, Multi-Hydro allows easy modelling of NBS by locally adapting the infiltration and storage capacities of the corresponding NBS and linking with their sizes and shapes.

In this study, a special green roof module of Multi-hydro is applied. This module is based on a linear reservoir structure (Versini et al., 2016) and is applied in the pixels that are defined as green roofs. In this module, the water content and the hydrological conductivity are assumed as constant in the green roof substrate. To be more specific, a simplified relationship of in/out for the fluctuation of the reservoir level is defined as follows:

$$H_r(t + \Delta t) = H_r(t) + R(t) - Q_{out}(t) \quad (1)$$

where $H_r(t)$ is the level of the reservoir (mm), Δt is the loop for each time step (3 min in this study), $R(t)$ refers to the rainfall rate (mm h^{-1}), and $Q_{out}(t)$ represents the runoff (mm) generated by the green roof at time *t*.

The $Q_{out}(t)$ is calculated with the following equation:

$$Q_{out}(t) = max\left[\frac{K_s \times \Delta t}{thick} \times (H_r(t) - fc \times thick), 0\right] \quad (2)$$

where K_s is the saturated hydraulic conductivity (mm s^{-1}), *thick* is the substrate thickness (mm), *fc* is the field capacity that adjusted by the substrate thickness and porosity.

The initial water level is defined at the first time step of the simulation:

$$H_r(0) = \phi \times thick \times IS \quad (3)$$

where ϕ is the porosity, and *IS* refers to the initial substrate saturation.

3. Numerical simulation of NBS scenarios

The numerical simulation process of NBS scenarios is shown in Fig. 5. Firstly, the land use data of the NBS scenarios and the raw DEM data are formatted by MH-AssimTool (i.e. a supplementary GIS tool for pre-treating the input data for Multi-Hydro, Richard et al., 2013) with the resolution of 10 m. During this format process, each pixel (10×10 m) is assigned a unique land use class with specifying its hydrologic and physical properties (see Qiu et al., 2021 for more details). This resolution is chosen because it is appropriate for representing the heterogeneity of the catchment and saving the calculation time. Here, the rainfall data, rasterised land use data, DEM data and sewer system data are used as the inputs to Multi-Hydro. Then, the Multi-Hydro surface model interacts with the drainage model. Finally, the outputs are presented by the flow in all conduits of the drainage system.

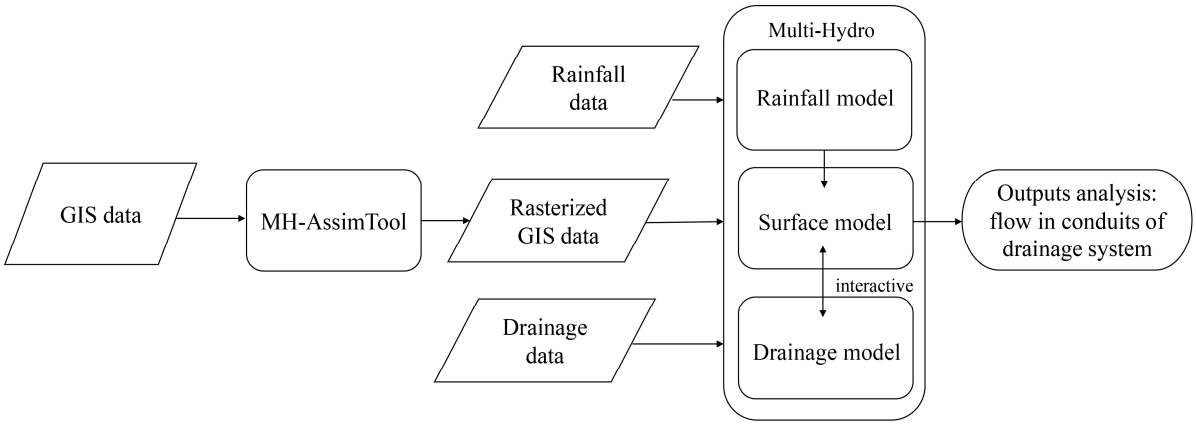

Fig. 5. The flow chart of numerical simulation of NBS scenarios.

3.1. Simulation scenarios

Baseline scenario

The baseline scenario is the current land use layout without any implementation of NBS. This scenario has been used to validate Multi-Hydro in the Guyancourt catchment (see Section 3.3 for more details) and used as a reference to compare with NBS scenarios.

NBS scenarios

Before introducing the scheme of creating NBS scenarios, it is significant to present the main characteristics of the studied NBS types. They are porous pavement (PP), rain garden (RG) and green roof (GR). PP is an infiltration-based measure with high porosity that can efficiently store and infiltrate surface runoff (Scholz and Grabowiecki, 2007). It can be applied on non-driveways (width $\leq$ 2.5 m), secondary driveways (2.5 m < width < 5 m), and parking lots. RG is a kind of artificial low-elevation/depressed greenbelt used to infiltrate surface runoff from surrounding impervious land uses. GR is a type of retention-based measure that a building's roof is partially or fully covered with vegetation. This study employed extensive GR and semi-extensive GR, consisting of a soil layer and a storage layer. The extensive one uses a relatively shallow growing medium ($\leq$ 10 cm) that fits well

on flat roofs and roofs with slopes (≤ 15°, Stanić et al., 2019), and the semi-intensive one contains a thick medium (= 20 cm) that is only suitable for flat roofs.

In order to assess the hydrologic and economic performances of the NBS scenarios, four sets of NBS scenarios are created based on the NBS characteristics and the current catchment conditions. Each set of NBS scenarios is described below.

The first set of NBS scenarios is designed to assess the performances of NBS with different implementation levels. Therefore, these NBS scenarios are created by up-scaling their implementation level in the whole catchment with the help of quantifying their fractal dimension (see Section 3.1.1 for more details on this scale invariance indicator). Taking the PP1 – PP4 scenarios as an example, based upon on the high-resolution land use data, we initially selected 0.147, 0.293, 0.440, 0.587 km^2 of the non-driveways and parking lots in the catchment (i.e. up-scaled by two times until all non-driveways and parking lots are selected), and then they were converted into PPs in PP1, PP2, PP3 and PP4 scenarios, respectively. As shown in Table 2, the fractal dimension (large-scale) of these four PP scenarios ranges from 1.60 to 1.77, indicating that the implementation levels of PPs are increased simultaneously across scales. The design procedure for other NBS scenarios follows a similar rule. For the RG scenarios, we selected the low elevation greenbelts around some houses and public buildings and converted them into RGs. For the GR scenarios, the buildings with impervious flat roofs and sloped roofs (slope ≤ 15°) are selected, and they are partially converted into extensive GRs in the GR1– GR4 scenarios.

The second set is the combined scenarios. In total, four different combined scenarios are created by performing the highest fractal dimension of the single type of NBS over the whole catchment (Table 2). For instance, the PP4+RG4+GR4 scenario is the combination of the scenarios of PP4, RG4

and GR4.

The third set of NBS scenarios is designed for assessing the performances of NBS at specific spatial locations. Here, two specific locations are selected and implemented with NBS, i.e. upstream and downstream. Indeed, the same type of NBS scenario (e.g. PP upstream and PP downstream) has the same total area over the whole catchment. However, both scenarios differ significantly in terms of spatial distributions of the considered asset, and the resulting fractal dimension is quite different.

The fourth set only contains the GR scenarios, and the purpose is to assess the performances of extensive and semi-intensive GRs concerning varying initial substrate conditions. More precisely, these GR scenarios are simulated with different substrate thicknesses and initial substrate saturation, but they have the same spatial layout and fractal dimension in the catchment to avoid the effects of spatial distributions and implementation levels of GRs. To maintain the same spatial layout for the extensive and semi-extensive GR scenarios, we selected only parts of the flat roofs to convert into GRs. The extensive GRs and semi-intensive GRs are supposed to have substrate thickness equal to 0.1 m and 0.2 m, respectively. Then, they are simulated with the initial substrate saturation as 10 %, 25 % and 50 %, respectively.

All details concerning the total areas, fractal dimensions, and implementation locations of the NBS scenarios are summarised in Table 2, and the resulting land use maps are illustrated in Fig. 6.

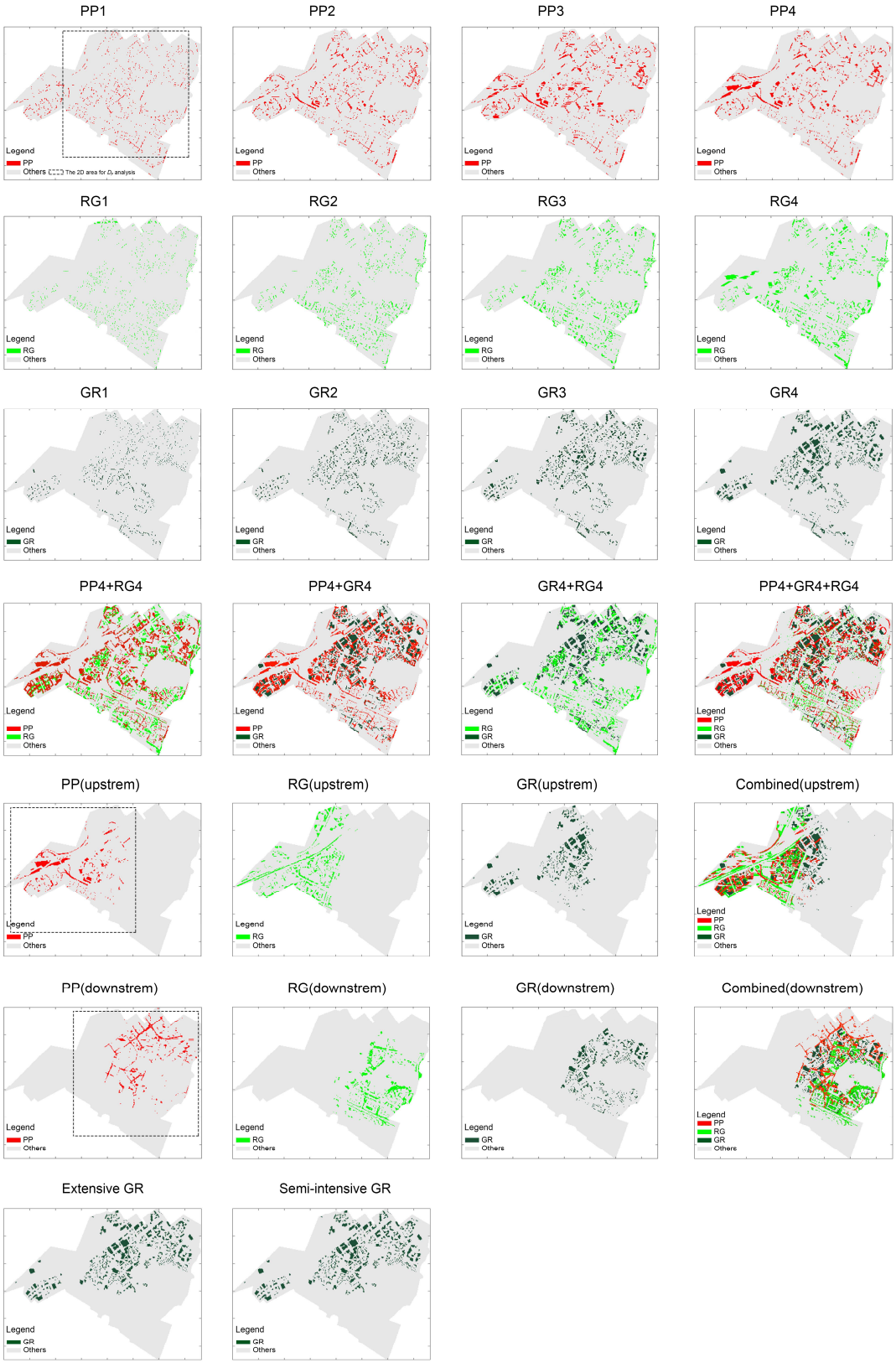

Fig. 6. Spatial layouts of all NBS scenarios.

Table 2. The details of the four sets of NBS scenarios.

NBS types	NBS scenario	Area (km^2)	D_F of NBS in small-scale/ large-scale range (after rasterization)	Description of scenarios
Porous pavement	PP1	0.147	0.42/1.6	PPs are implemented on some non-driveways and parking lots.
	PP2	0.293	0.73/1.64	
	PP3	0.440	0.9/1.68	
	PP4	0.587	1.1/1.77	PPs are implemented on all non-driveways and parking lots.
Rain garden	RG1	0.108	0.24/1.54	Low elevation greenbelts around some houses and public buildings are converted into RGs.
	RG2	0.215	0.59/1.59	
	RG3	0.323	0.79/1.61	
	RG4	0.430	0.95/1.64	Low elevation greenbelts around all houses and some public buildings are converted into RGs.
Green roof	GR1	0.119	0.42/1.53	Some impervious flat roofs and roofs with light slope (≤ 15°) are converted into extensive GRs.
	GR2	0.239	0.67/1.59	
	GR3	0.358	0.85/1.60	
	GR4	0.478	1.03/1.61	All impervious flat roofs and some roofs with light slope (≤ 15°) are converted into extensive GRs.
Porous pavement and rain garden	PP4+RG4	1.017	1.26/1.78	A combination of GR4 and RG4 scenarios.
Porous pavement and green roof	PP4+GR4	1.065	1.28/1.79	A combination of PP4 and GR4 scenarios.
Rain garden and green	RG4+GR4	0.908	1.19/1.74	A combination of RG4 and GR4 scenarios.

NBS types	NBS scenario	Area (km^2)	D_F of NBS in small-scale/ large-scale range (after rasterization)	Description of scenarios
roof				
Porous pavement, rain garden and green roof	PP4+RG4+GR4	1.495	1.31/1.80	A combination of PP4, RG4 and GR4 scenarios.
Porous pavement	PP (upstream)	0.183	0.99/1.47	PPs are implemented on some non-driveways, secondary roads, and parking lots that located upstream of the catchment.
	PP (downstream)	0.183	0.93/1.49	PPs are implemented on some non-driveways, secondary roads, and parking lots that located downstream of the catchment.
Rain garden	RG (upstream)	0.430	0.95/1.53	RGs are implemented on some upstream low elevation greenbelts around public buildings.
	RG (downstream)	0.430	1.05/1.5	RGs are implemented on some downstream low elevation greenbelts around houses and public buildings.
Green roof	GR (upstream)	0.253	1.08/1.48	GRs are implemented on upstream impervious flat roofs and the roofs with slightly slope (≤15°).
	GR (downstream)	0.253	1.0/1.53	GRs are implemented on downstream impervious flat roofs and the roofs with slightly slope (≤15°).
Porous pavement, rain garden and green roof	Combined (upstream)	0.867	1.44/1.68	A combination of PP (upstream), RG (upstream) and GR (upstream) scenarios.
	Combined (downstream)	0.867	1.4/1.69	A combination of PP (downstream), RG (downstream)

NBS types	NBS scenario	Area (km^2)	D_F of NBS in small-scale/ large-scale range (after rasterization)	Description of scenarios
				and GR (downstream) scenarios.
Green roof	Extensive GR	0.441	1.07/1.56	Extensive GRs and Semi-intensive GRs are implemented on some impervious flat roofs.
	Semi-intensive GR	0.441	1.07/1.56	

3.1.1. Fractal dimension of NBS scenarios

To describe and quantify the multiscale implementation levels and heterogeneous spatial distributions of NBS in the four series of NBS scenarios, conventional assessment tools (e.g. percentage, proportion) are not appropriate because they take the mean occupation of NBS rather than their morphological arrangement. Hence, it is important to introduce the fractal dimension (D_F), which relies on the scale invariance concept that assumes similar features can be observed from the smallest scale to the largest scale.

The concept of fractal was first proposed by Mandelbrot (1983), and after widely used in various science fields (Schertzer and Lovejoy, 1987; Ichiba et al., 2018; Qiu et al., 2021). For fractal objects or sets, the dimension is called D_F. In this study, an easier method called box-counting (Lovejoy et al., 1987) was applied to compute the D_F of the NBS scenarios. Firstly, considering a geometrical object (here is presented as a NBS) of outer scale L observed in a range of scales l (i.e. pixels with the size of l). Then, the resolution λ is defined as $\lambda = \frac{L}{l}$. Defining $N_{\lambda,A}$ is the number of non-overlapping pixels of size l to cover the geometrical set A. For a fractal field, when $\lambda \to \infty$, there is a power-law relation between the fractal dimension and the number of "non-empty" pixels of

the $N_{\lambda,A}$ at the resolution λ:

$$N_{\lambda,A} \approx \lambda^{D_F} \tag{4}$$

where $\approx$ means the asymptotic equivalence.

In practice, firstly, counting the number of non-empty pixels at the pixel size of l, then up-scaling the pixel size by the power of two at each step (i.e. 4 by 4 adjoined pixels are merged in our 2D space). Then, counting again the number of non-empty pixels at the new resolution, and repeat this process until reaching the maximum pixel size *L*. At each resolution, the numbers of non-empty pixels $N_{\lambda,A}$ are counted, and they are displayed in a log-log plot. For a fractal set, the points of this plot will be along a straight line. Based on Eq. (4), the fractal dimension D_F can be estimated as its slope (Eq. 5).

$$D_F \approx \frac{\ln(N_{\lambda,A})}{\ln \lambda} \tag{5}$$

Here, for each scenario, a square area of 256 x 256 pixels was extracted from the catchment to make the fractal analysis (see the example of the PP1 scenario in Fig. 6). To maximum selected all pixels representing NBS, this square area is the greatest possible size characterised by a multiple of two in the studied catchment. For the third set of NBS scenarios, the location of the selected square is different from the other set of NBS scenarios because of the specific spatial layout of the NBS (see the example of the PP upstream and downstream scenarios in Fig. 6).

The D_F of the four sets of NBS scenarios are summarised in Table 2, and the corresponding figures are shown in Fig. 7. Here, all NBS scenarios are characterised by two scaling behaviour regimes, with a scale break roughly at 40 m. For each regime, the scaling is robust, with the coefficient of determination (r^2) of linear regression around 0.99. The first regime corresponds to the small-scale range (10 – 40 m, presented in the red line in Fig. 7) that related to the intrinsic 2D size

of the NBS, which means that the NBS performed on the selected areas (i.e. roads, buildings and low-elevation green belts) with sizes ranging between 100 m^2 and 1600 m^2. In this observation scale, the D_F of the four sets of NBS scenarios ranges from 0.24 to 1.4.

Regarding the large-scale range (40 – 2560 m), it typically presents the spatial distributions and implementation levels of NBS in the catchment. Generally, it noticed that the D_F of all NBS scenarios in this range of scales tends to be 2 (the dimension of the 2D space studied). However, as the NBS are embedded in the environmental context that containing other types of land use (e.g. parking, water, green space), it exhibits a scaling behaviour with the D_F of all NBS scenarios are less than 2. For instance, the D_F (large-scale range) of the second set of NBS scenarios ranging from 1.74 to 1.8, namely, the spaces are largely filled by NBS in this observation scale.

Overall, it noticed that the D_F of the NBS scenarios in small-scale and large-scale range increases with increasing the proportion of the NBS implementation in the catchment, which presents that the D_F can reflect the implementation level of NBS over a wide range of scales. Indeed, such a scale invariance indicator contains the information across scales and represents the space heterogeneity of NBS in the catchment, while the initial percentage defined at the maximum resolution is not able to present the heterogeneous spatial distribution of NBS explicitly.

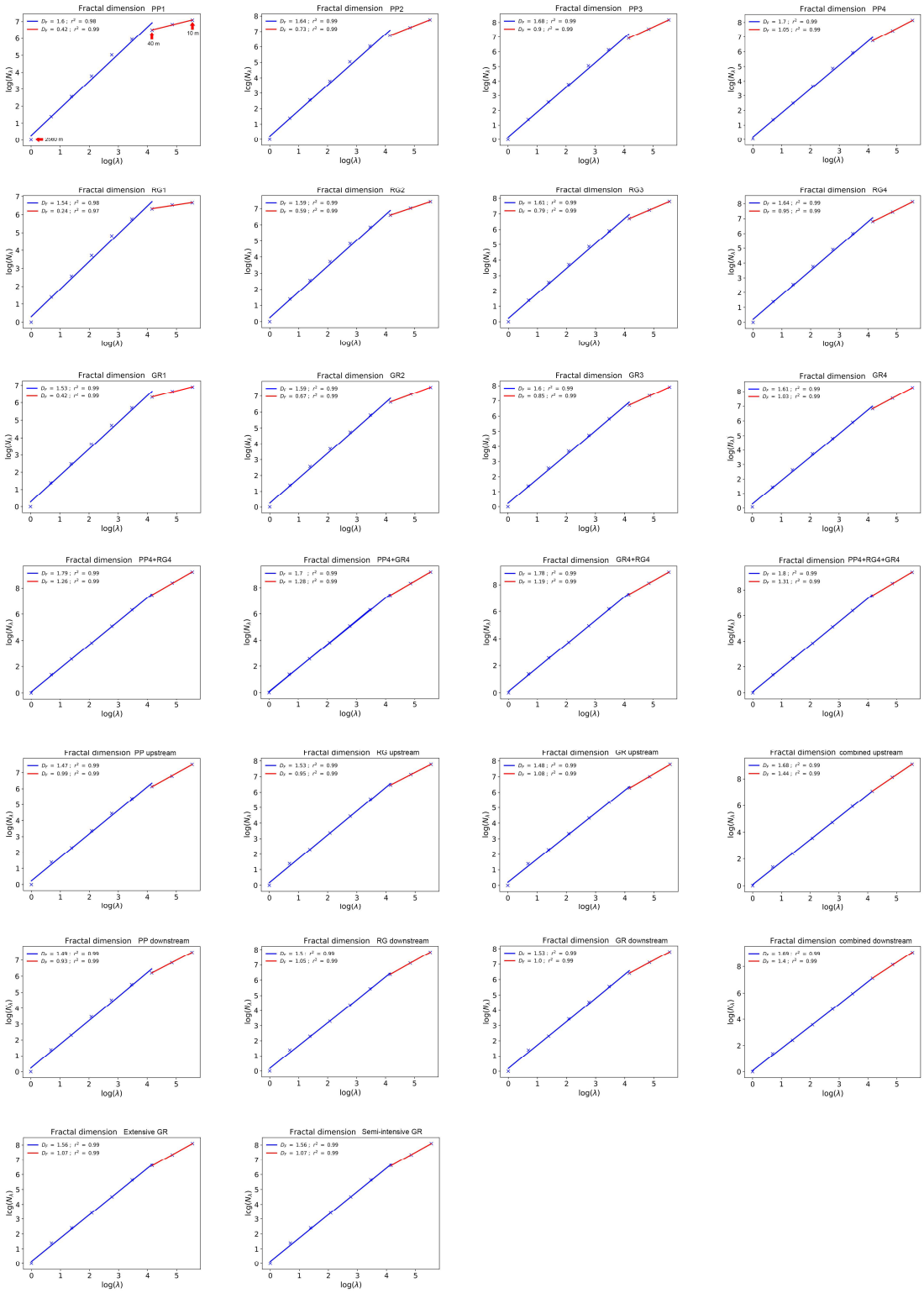

Fig. 7. Fractal dimension of NBS scenarios (the red line represents the small-scale range (10 – 40 m), and the blue line corresponds to the large-scale range (40 – 2560 m)).

3.2. Parameterization of NBS

The standard parameters (i.e. hydraulic conductivity, capillary suction, moisture deficit, manning's coefficient, depth of interception) for representing a land use class are selected from the Multi-Hydro manual (Giangola-murzyn, 2013).

As NBS are specific land uses, they are characterised with different retention/storage capacity, the corresponding parameters (e.g. thickness, porosity) are based on the literature (more details about these parameters can be found in Qiu et al., 2021) and experimental sites (Versini et al., 2016; Stanić et al., 2019). The RGs and PPs are simulated with the associated storage capacity around 300 L m^{-2} and 74 L m^{-2}, respectively. Here, it needs to mention that five initial parameters are set for GR scenarios (Table 3). For the first set of GR scenarios (GR1-GR4), the *thick*, *IS*, ϕ, *fc*, and hydraulic conductivity is 0.05 m, 10 %, 0.395, 0.2, and 1.2 m s^{-1}, respectively. For the extensive and semi-intensive GR scenarios, the ϕ and the hydraulic conductivity are set the same with 0.395 and 1.2 m s^{-1},the *thick* and *IS* have been mentioned in Section 3.1, and the *fc* is 0.39 and 0.79, respectively.

Table 3. The selected parameters for different GR scenarios.

Scenario	Substrate thickness (m)	Initial substrate saturation	Porosity	Hydraulic conductivity (m s^{-1})	Field capacity
GR1 – GR4	0.05	10 %	0.395	1.2	0.2
Extensive GR	0.1	10 %/25 %/50 %	0.395	1.2	0.39
Semi-intensive GR	0.2	10 %/25 %/50 %	0.395	1.2	0.79

3.3 Model validation

Because the Multi-Hydro has been validated in Guyancourt catchment by comparison of the

water levels (m) measured at the gauge of the storage basin (outlet: Etang de Roussières) with the simulated ones under the three long rainfall events of 2015 (described in Section 2.2, Qiu et al., 2021), here only some basic information is presented.

As shown in Fig. 8, the simulated water levels are highly consistent with the observed ones under the three rainfall events, only a slight underestimation of the observed water levels between 7 and 20 hours under the 12/09/2015 event. The reason might be related to the spatial variability of the rainfall that the rainfall intensity in the measurement location was underestimated. The model performance was evaluated through two indicators: Nash-Sutcliffe Efficiency (NSE $\leq$ 1, Nash and Sutcliffe, 1970) and Percentage Error (PE, Moriasi et al., 2007). For the three rainfall events, the NSE value is 0.926, 0.929, and 0.954, respectively. Correspondingly, that of the PE value is 4.6 %, 2.2 % and 3.9 %, respectively. Overall, these results confirmed that the Multi-Hydro model performs sufficiently reliable to represent the heterogeneity of the catchment, and hence it is appropriate to assess the hydrological responses of different NBS scenarios under different rainfall conditions.

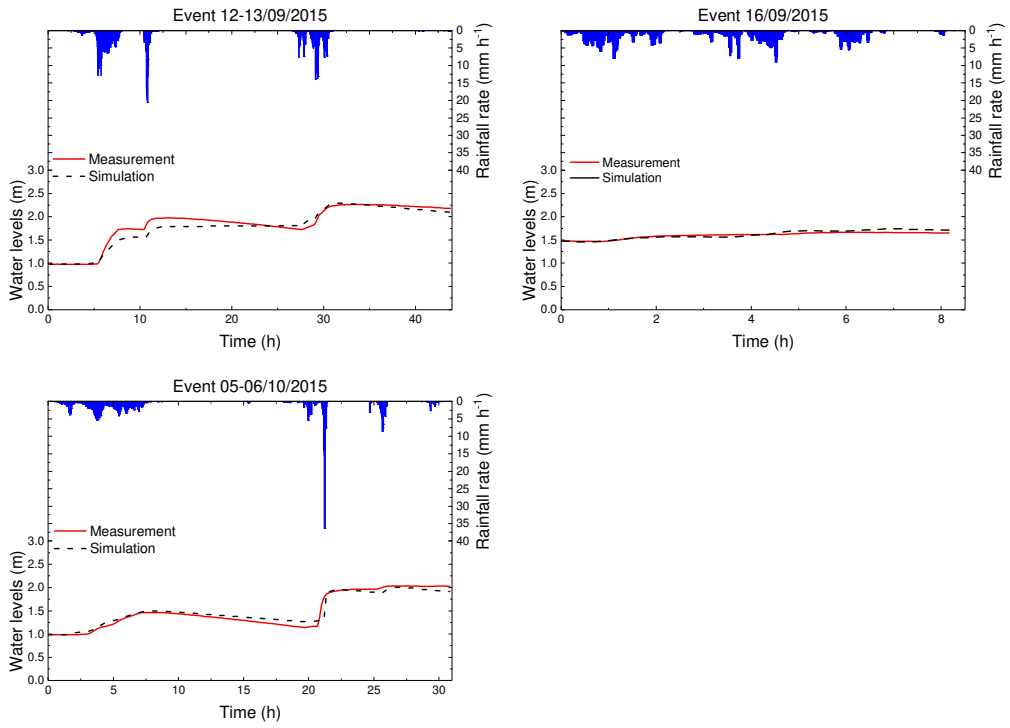

Fig. 8. Comparison of the observed and simulated water levels of the baseline scenario under three rainfall events of 12-13/09/2015, 16/09/2015 and 05-06/10/2015.

4. Evaluation indicators

In this study, two different types of evaluation indicators are integrated for assessing the cost-effectiveness of NBS scenarios: (i) the technical indicator (i.e. reduction of peak flow and total runoff volume) used for evaluating the hydrological performances of NBS, and (ii) the economic indicator (i.e. LCC) used for assessing the economic costs of NBS scenarios.

4.1. Technical indicators

The hydrological performances of NBS are firstly assessed in terms of the simulated flow in all conduits (in total 4474) of the drainage system (the right side of Fig. 2). To consider the flow in all conduits is to comprehensively investigate the impact on any conduit of the drainage network. Then, a percentage error was computed between the baseline scenario and each NBS scenario. In detail,

two indictors, reduction of peak flow (ΔQ_{p}) and total runoff volume (ΔV), are considered. These two indicators are computed with the following equations:

$$\Delta Q_{\mathrm{p}}(\%) = \frac{Q_{\mathrm{p_{base}}} - Q_{\mathrm{p_{NBS}}}}{Q_{\mathrm{p_{base}}}} \times 100 \quad (6)$$

$$\Delta V(\%) = \frac{V_{\mathrm{base}} - V_{\mathrm{NBS}}}{V_{\mathrm{base}}} \times 100 \quad (7)$$

where $Q_{\mathrm{p_{base}}}$ and V_{base} refer to the peak flow and total runoff volume of the baseline scenario, respectively. Correspondingly, $Q_{\mathrm{p_{NBS}}}$and V_{NBS} are those for NBS scenarios, respectively.

4.2. Economic indicator

Life cycle costs is an economic indicator for evaluating the performances of NBS scenarios with considering all the related costs throughout the lifetime of NBS (Spatari et al., 2011). In detail, three stages in terms of construction, operation, and the end of life should be taken into consideration (Fuller and Petersen, 1996). The associated cost corresponding to the three stages: (i) the capital expenses; (ii) operation and maintenance expenses; and (iii) salvage value.

In order to consider all the related costs, a transformation is required based on a proper discount rate. The present value of cost (PVC) is applied to compute the LCC with the following equation:

$$\mathrm{PVC} = C_0 + \left(\frac{C_a\left((1+r)^{T+1}-1\right)}{r(1+r)^T}\right) - \frac{SV}{(1+r)^T} \quad (8)$$

where PVC is the present value of LCC of NBS (€/m^2), C_0 and C_a represent the capital cost (€/m^2) and the annual operation and maintenance cost (€/m^2), respectively; T is the lifespan (year), r refers to the discounting rate (5 % in this study), and SV is the salvage value at the end of the year of the lifespan (€/m^2).

The salvage value (SV) refers to the residual life of NBS at the end of their lifespan. The residual life of NBS needs to be considered because NBS may not be entirely exhausted at the end of

the design year. The SV is computed by using the following equation:

$$SV = \left(1 - \frac{L_A}{T}\right) \times C_a \quad (9)$$

where L_A is the time span from the year of last maintenance to the end of the year of lifespan (generally, NBS are maintained at each year, thus, L_A is equal to 1 in this study).

4.3. Cost-effectiveness evaluation

The evaluation process of cost-effectiveness of NBS scenarios takes into account the equilibrate weight of two technical indicators (ΔQ_{p} and ΔV) and the economic indicator of LCC by using the following equation:

$$\mathrm{CE} = \frac{(\Delta Q_{\mathrm{P}} + \Delta V)/2}{\mathrm{PVC} \times A_{\mathrm{NBS}}} \quad (10)$$

where A_{NBS} (m^2) is the total implementation area of NBS in each NBS scenario.

5. Results and discussion

In this study, the local reductions of peak flow and total runoff volume of each set of NBS scenarios are presented with the box-plots regarding the flow in all the conduits (4470) of the drainage system.

5.1. Different implementation levels of NBS scenarios

As shown in Figs. 9 and 10, a similar result can be found for the first set of NBS scenarios under the eight studied rainfall events: the ΔQ_{p} and ΔV are generally positive linearly related to the D_F of NBS scenarios. Namely, the hydrological performances of NBS scenarios increase with the increasing of implementation level of NBS. However, each type of NBS scenario has some specific performances, which can be summarised as follows:

(i) For PP1 – PP4 scenarios, it is worth mentioning that the largest mean value of ΔV is

computed for the PP4 (D_F =1.77 in large-scale) under the EV1, which is around 7 % higher than that of the other PP scenarios (D_F <1.7 in large-scale). Namely, in this short and weak rainfall event, the hydrological performance of PPs is significantly increased with increasing their D_F.

(ii) Concerning the RG1 – RG4 scenarios, enlarging the D_F of RGs over the whole catchment is not significant for increasing the hydrological performances of the RG scenarios (i.e. the average difference of ΔQ_p and ΔV between each RG scenario is less than 2 %). Furthermore, the relationship between the hydrological performances (ΔQ_p and ΔV) of RGs and their D_F is not merely positive linearly in EV7. The mean values of these two indicators of the RG3 scenario are around 0.8 – 1 % lower than that of the RG2 scenario. The reason can be related to the spatial layout of the RGs and the convey capacity of the conduits for flow routing, which some relevant conduits may overload in this rainfall event. This result is consistent with some previous studies (Fry and Maxwell, 2017; Ercolani et al., 2018), which have shown that the relationship between peak flow reduction and NBS percentage conversions is non-linear if 25 % of conduits exceeding 80 % of filling.

(iii) Concerning the two stronger rainfall events (EV2 and EV8, return period larger than one year), the mean values of ΔQ_p and ΔV of each GR scenario are lower than 20 %, even the scenario characterised with the highest D_F (large-scale > 1.6). This result is generally consistent with the previous studies, which has been shown that GRs are more effective for the smaller storms (Palla and Gnecco, 2015; Ercolani et al., 2018).

Comparing the hydrological responses of each NBS scenario, which varies depending on the

rainfall event. In our modelling experiments, the performances of PP scenarios are relatively less effective than that of the RG and GR scenarios, especially in some stronger rainfall events. The relationship between the performances of the NBS scenarios and the rainfall intensities, some non-linearity responses were found. Our study suggests that this non-linearity could be related to the intersection effects of both spatial variability in rainfall and NBS distributions. Qiu et al. (2021) has used the multifractal intersection theorem to indicate that the rainfall spikes may intersect more often elsewhere than on NBS. Therefore, the potential performances of NBS can be biased due to the less intersection between the extremes of rainfall and NBS.

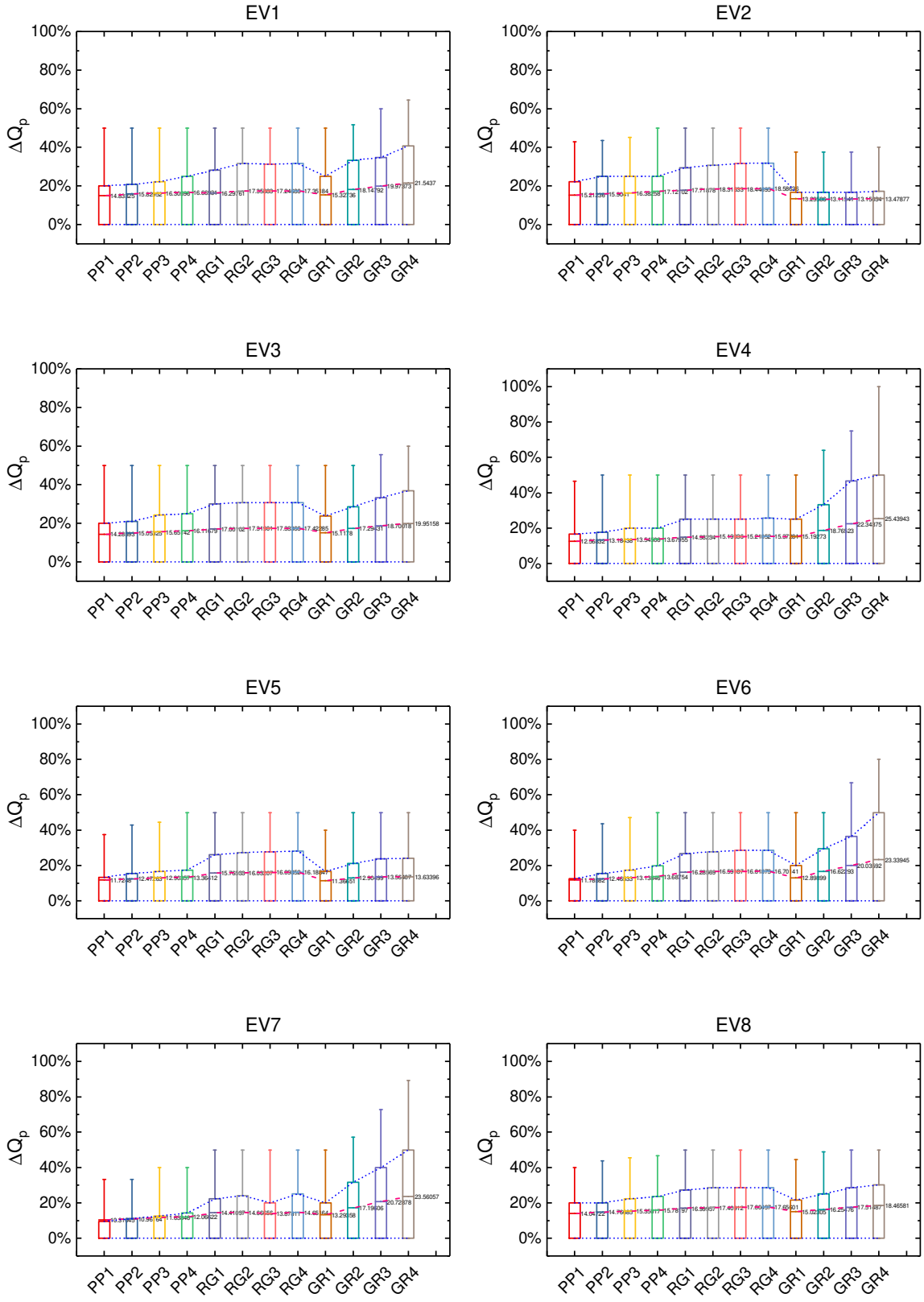

Fig. 9. Peak flow reduction of the first set of NBS scenarios under the eight rainfall events.

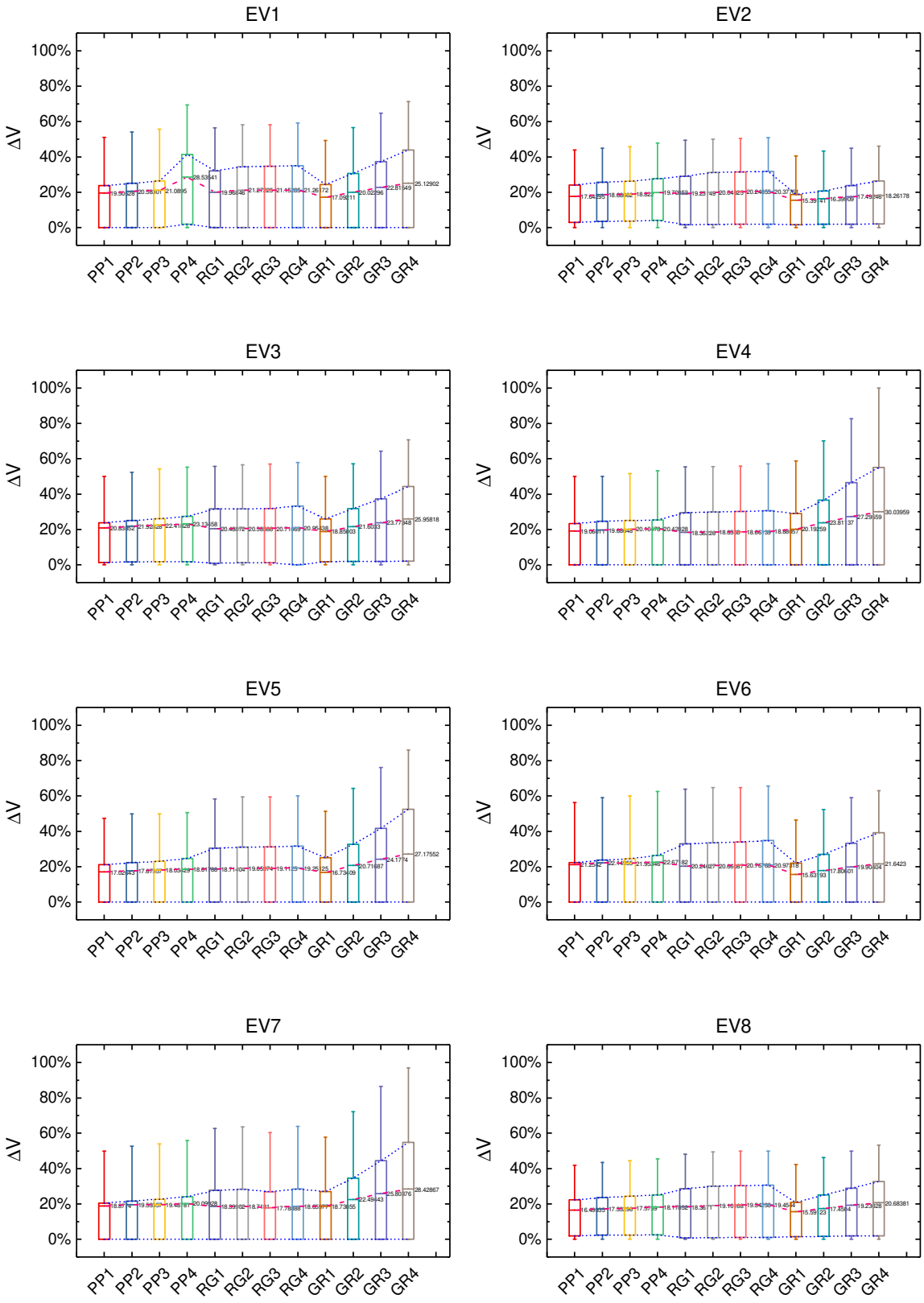

Fig. 10. Total runoff volume reduction of the first set of NBS scenarios under the eight rainfall

events.

5.2. Combined scenarios

As shown in Figs. 11 and 12, among the four combined scenarios, the combination of three types of NBS has the best performance concerning the peak flow and total runoff volume reduction because of the highest D_F, and this result is generally consistent with some previous studies (Ahiablame et al., 2013). For the eight studied rainfall events, the mean values of ΔQ_p of PP4+RG4+GR4 scenario range from 26.8 % to 44 %, and that of the ΔV range between 35.1 % and 48.3 %. Concerning the three other combined scenarios, the performances of the PP4+GR4 scenario are better than the two others, especially in some rainfall events with a relatively lower spatial variability. The mean values of ΔQ_p of PP4+GR4 scenario range from 25.6 % to 37.3 %, and that of the ΔV range between 33.1 % and 41.3 %. The reason could be related to the PP4+GR4 is characterised by a relatively higher D_F, and the locations of RGs may not highly intersect with the rainfall spikes in some rainfall events.

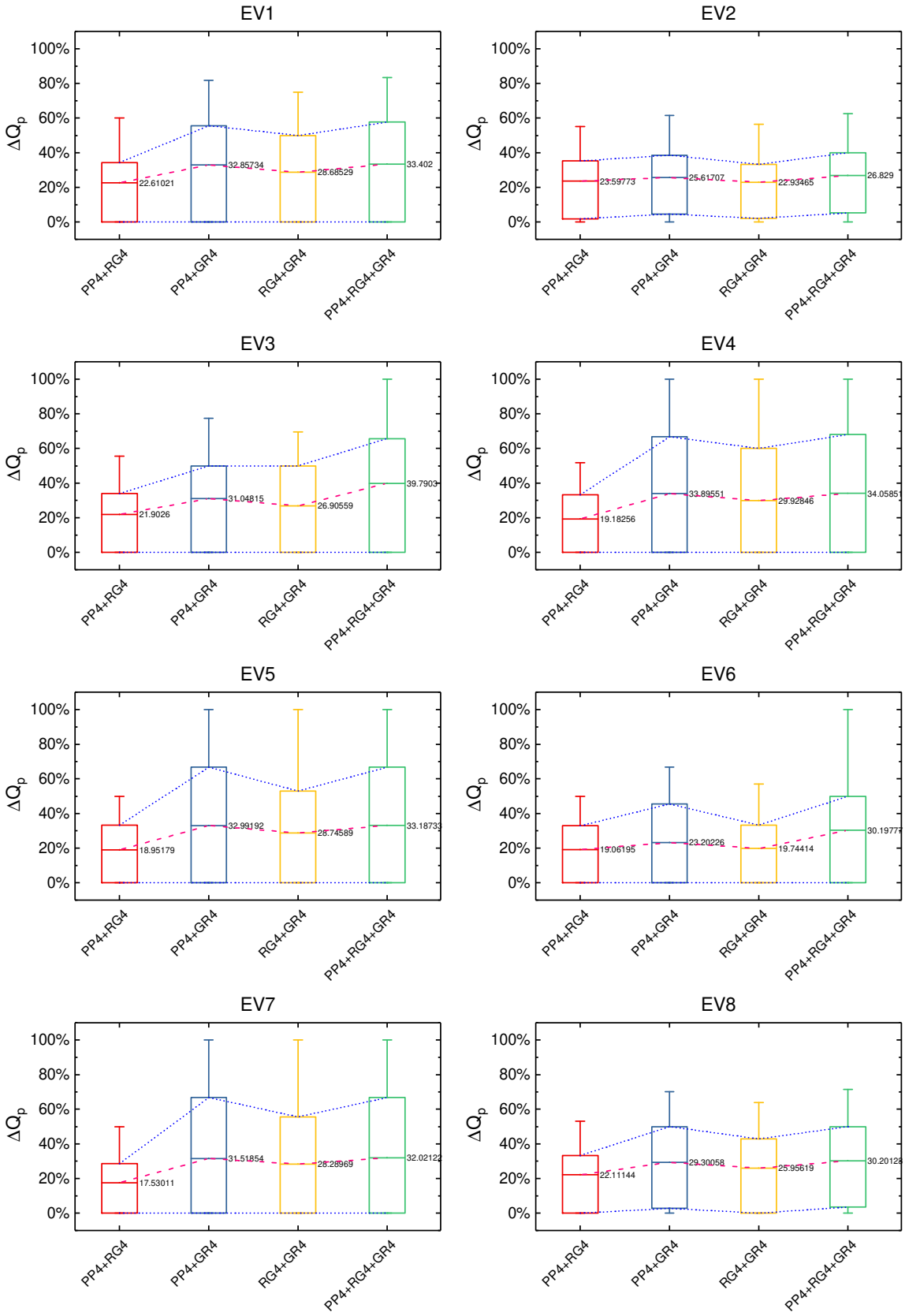

Fig. 11. Peak flow reduction of the second set of NBS scenarios under the eight rainfall events.

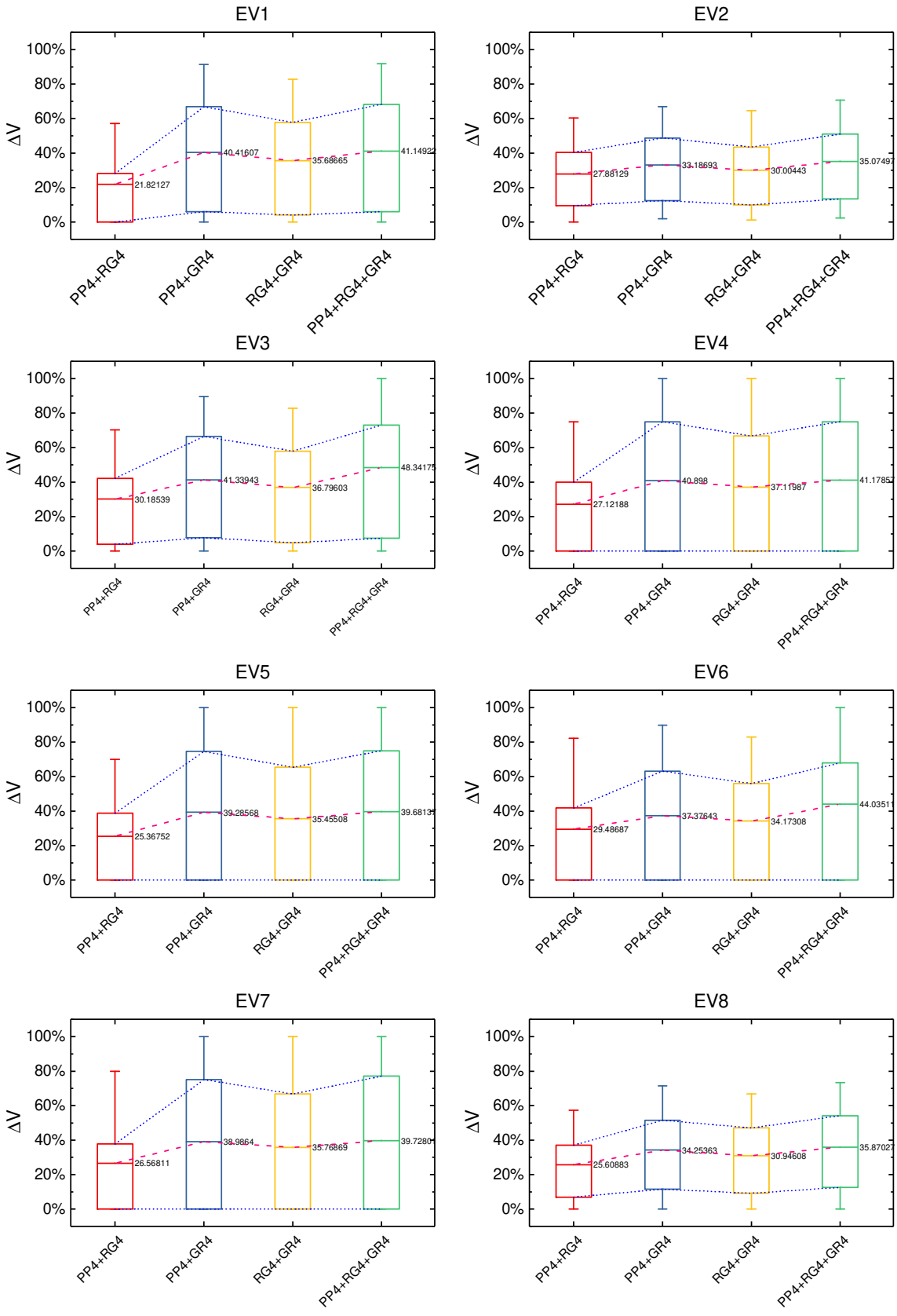

Fig. 12. Total runoff volume reduction of the second set of NBS scenarios under the eight rainfall

events.

5.3. Location analysis of NBS scenarios

One of the significant advantages of Multi-Hydro is its ability to represent the spatial layout of NBS accurately with a high resolution. Therefore, a location analysis of the third set of NBS scenarios under the EV8 is adopted. The reason for only selecting EV8 is that this event has the strongest rainfall intensity, and the spatial variability of this event is more pronounced than that of the other event.

The results of the two hydrological indicators of each NBS scenario are shown in Fig. 13, and several findings can be summarised as follows:

(i) The scenarios with performing NBS downstream of the catchment have better performances than those by implementing NBS upstream. The reason can also be related to the intersection effects of the spatial variability in rainfall and NBS distributions. As shown in Fig. 4, for EV8, the upstream accumulated rainfall is stronger than that of the downstream. Hence, the NBS located in these areas may more easily be saturated. Furthermore, the downstream is the drained area that near to the outlet, and the NBS implemented in these areas can be more effective to reduce the runoff. A similar finding was indicated by some previous studies, which suggested that the peak flow and total runoff volume can be reduced more significantly at the outlet of the catchment (Helmi et al., 2019).

(ii) GR downstream scenario is the most effective one, with the mean values of ΔQ_p around 44 % and ΔV around 46 %, followed by the two PP scenarios. The hydrological performances of PP upstream and PP downstream scenarios are similar, and the reason may be related to these two scenarios have very similar D_F. The two RG scenarios are less effective, with ΔQ_p and ΔV around 20 % lower than that of the GR and PP scenarios.

(iii) The mean values of ΔQ_p and ΔV of two combined scenarios are around 30 %, which is less effective compared to the two GR and PP scenarios. The reason can be related to RGs are less intersected with the strong rainfall cells, and finally reduces the overall performances of combined scenarios (see Fig. 6 for the spatial distributions of RGs).

Overall, these results indicated that with a careful arrangement of a single type of NBS in space, a substantial reduction of peak flow and total runoff volume can be achieved.

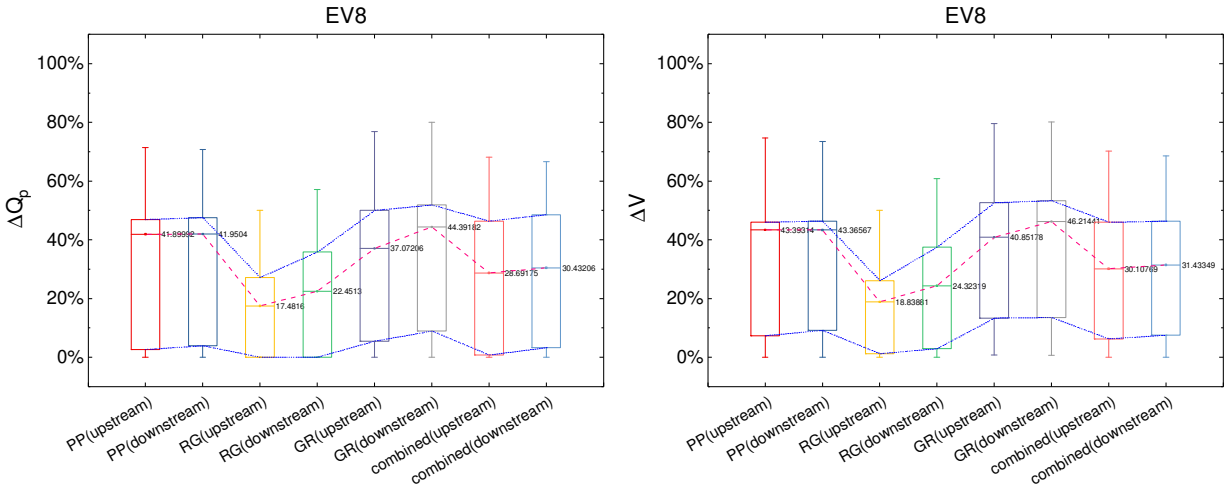

Fig. 13. Peak flow reduction and total runoff volume reduction of the third set of NBS scenarios under the EV8.

5.4. The different properties of GR scenarios

As described in Section 3.1, the extensive GR and semi-intensive GR are studied. For the eight rainfall events, the two types of GR scenarios with the *IS* of 10 % and 25 % have similar performances: the mean values of ΔQ_p and ΔV are almost unvaried (see Figs. 14 and 15). However, when the *IS* increases to 50 %, the mean values of ΔQ_p of extensive GR scenario range from 10.7 % to 25.4 %, and the corresponding semi-intensive GR scenario range from 20.7 % to 25.7 %. For the mean values of ΔV, the extensive GR scenario with the *IS* of 50 % is averagely around 3 % lower

than that of the semi-intensive GR scenario. The largest difference of the mean values of ΔQ_p and ΔV between two types of GR scenarios is found in EV6, which is 10 % and 7.3 %, respectively. The reason is that this rainfall event consecutively lasts around 2 hours, which the extensive GRs with *IS* of 50 % are more easily be saturated. Overall, the mean values of ΔQ_p and ΔV of the semi-intensive GR scenario (*IS* = 50%) are higher than that of the extensive GR scenario (*IS* = 50%) under the stronger rainfall events (return period larger than 1 year). However, the performances of the two types of GR scenarios (*IS* = 10 %, 25 % and 50 %) have no difference under some weak rainfall events (return period $<$ 1 month). Therefore, these results reveal that the semi-intensive GR is only more effective than the extensive GR in strong rainfall events.

In total, the results indicated that the *IS* of GR is more sensitive than their substrate thickness. The hydrological performances of the semi-intensive GR scenario are only more effective than the extensive GR scenario with the *IS* reach of 50 %.

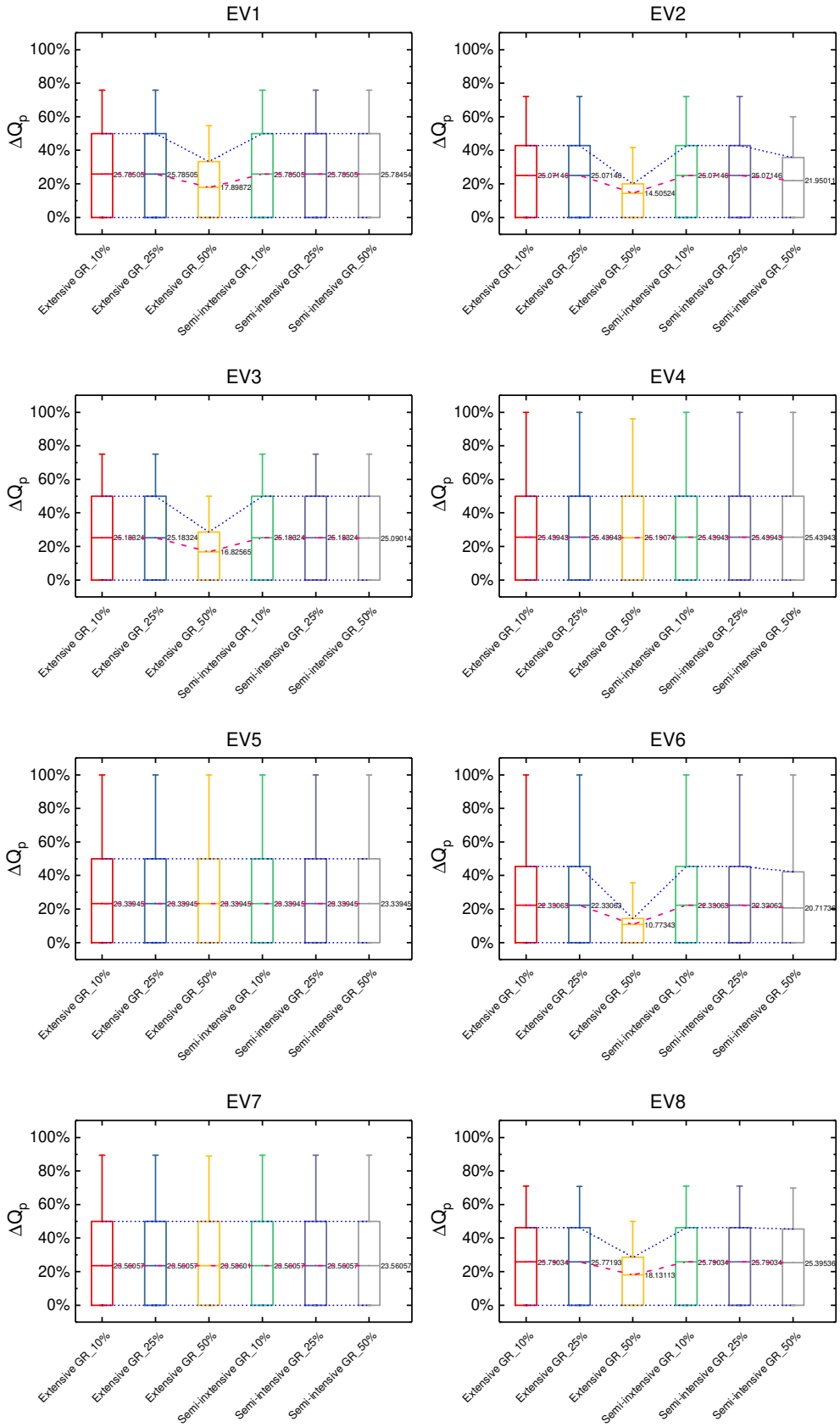

Fig. 14. Peak flow reduction of the fourth set of NBS scenarios under the eight rainfall events.

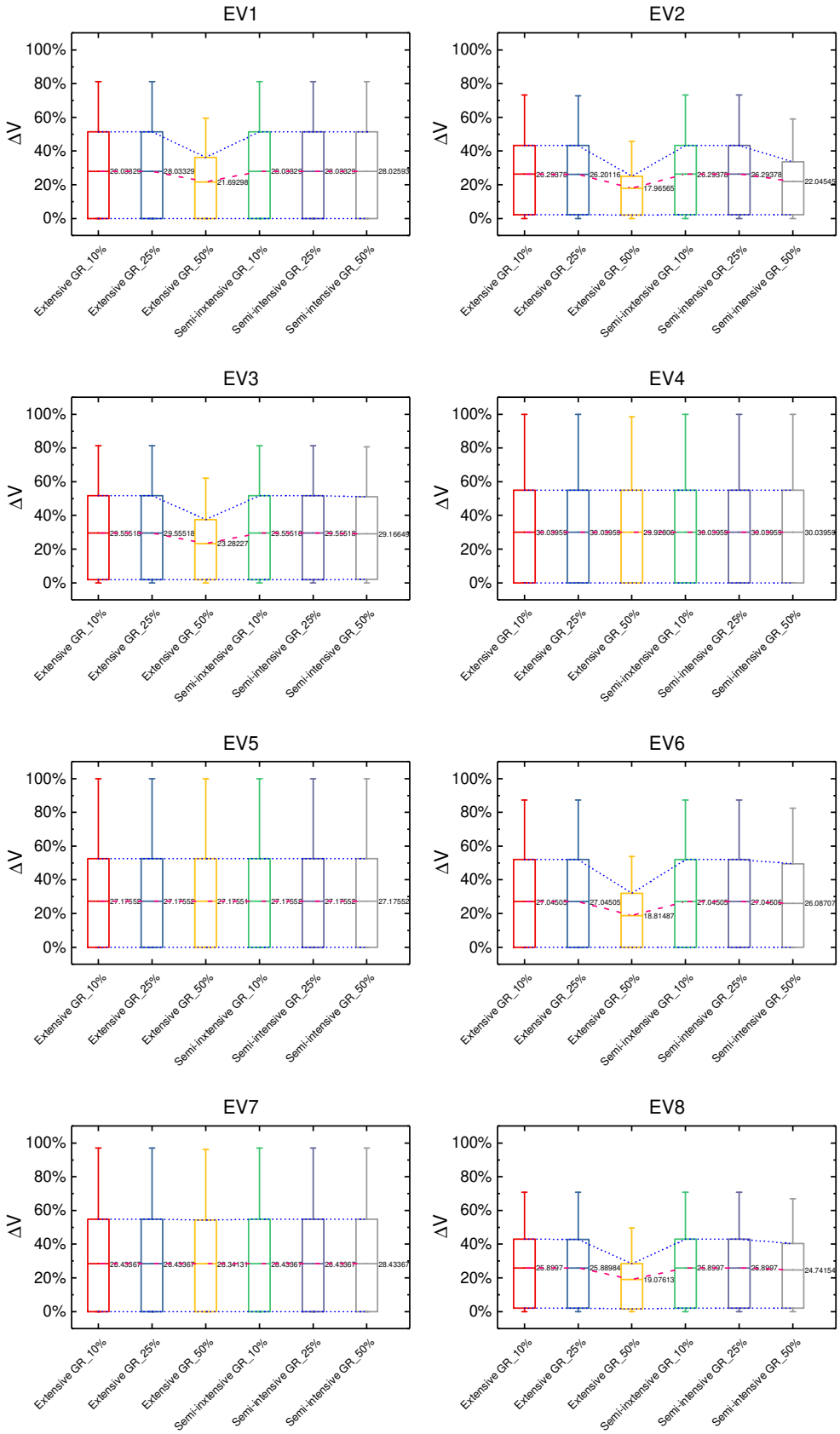

Fig. 15. Total runoff volume reduction of the fourth set of NBS scenarios under the eight rainfall

events.

5.5. Life cycle costs analysis

In this study, based on the grid-based character of Multi-Hydro, the total implementation areas of NBS can be calculated by counting the pixels that represent the NBS (as mentioned in Section 3, a unique NBS is assigned to each pixel). The PVC of each scenario is calculated based on Eq. (8), and the relative parameters (i.e. empirical cost, life span, and annual operation and maintenance costs) are obtained from the literature (more details of these parameters can be found in Table 4). The analysis period is considered for one life cycle of NBS. Taking the extensive GR as an example, the life span of the extensive GR is estimated as 40 years with respect to the doubling of the impervious roof life span because the vegetation cover protects the membrane from physical damage (Carter and Keeler, 2008). All extensive GR is considered implemented at the year zero, and a standard discount rate of 5 % was applied (Liao et al., 2018). The construction costs of an extensive GR system were taken from the literature (Leimgruber et al., 2019), which is 35 €/m^2, and the operation and maintenance on an extensive GR are considered for each year, around 1.75 €/m^2. The estimated PVC of other studied NBS are somewhat following a similar rule. The life span of PP is 20 years, which is lower than that other the other NBS due to the impact of clogging (Li et al., 2020).

Here, the PVC (€/m^2) of each type of NBS is shown in Fig. 16 (a), the highest PVC was computed for the semi-intensive GR, around 154.4 €/m^2. Correspondingly, the lowest one is RG, with the PVC around 57 €/m^2. The corresponding LCC (million €) of each NBS scenario is determined by $\mathrm{PVC} \times A_{NBS}$, which is shown in Fig. 16 (b). Concerning the LCC of each NBS scenario, the combined scenarios are much higher than the scenarios with single types of NBS. For instance, the PP4+RG4+GR4 scenario has the highest LCC, which is around 93.5 million €.

Correspondingly, the RG1 scenario has the lowest LCC, which is approximately 6.1 million €.

Table 4. The parameters of PVC of each type of NBS.

NBS type	Construction cost (C_0) (€/m^2)	Annual operation and maintenance Costs (C_a) (€/m^2)	Life span (T) (year)	Discount rate (r)	Reference
Porous pavement	49.4	1.07	20	5%	Praticò et al., 2015; Montalto et al., 2007; Li et al., 2020
Rain garden	30	1.5	40	5%	Leimgruber et al., 2019
Extensive GR	35	1.75	40	5%	Leimgruber et al., 2019
Semi-intensive GR	120	1.91	40	5%	www.travaux.com/couverture-toiture/guide-des-prix/combien-coute-une-toiture-vegetalisee

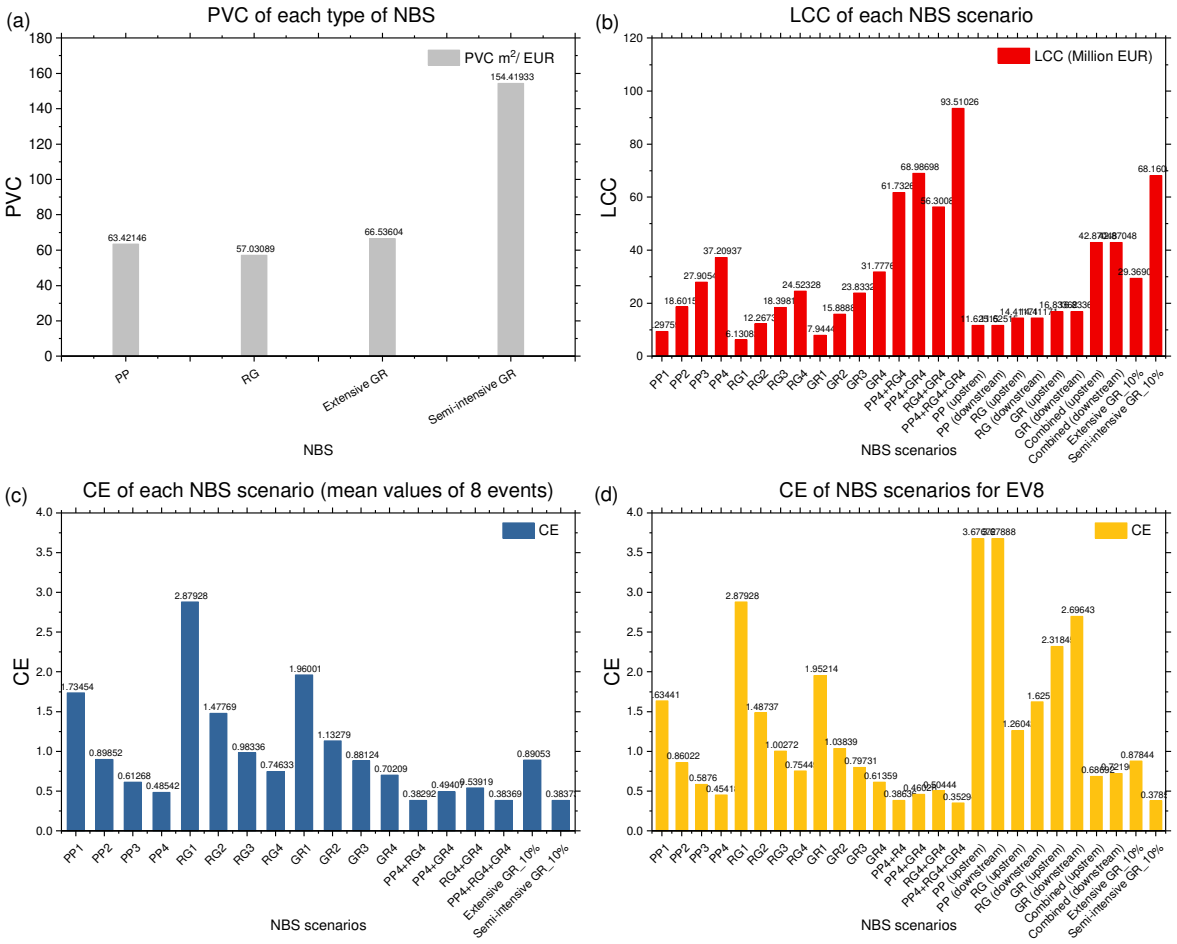

Fig. 16. (a) PVC of each type of NBS; (b) LCC of each NBS scenario; (c) The mean values of CE of

each NBS scenario; (d) CE of each NBS scenario under EV8.

5.6. Cost-effectiveness evaluation

The cost-effective evaluation of NBS scenarios is based on the Eq. (10), then the mean values of CE of each scenario (except for the third set of NBS scenarios) under the eight rainfall events are taken into account. Here, the larger the CE values, the closer the related scenario is to the optimal solution.

As shown in Fig. 16 (c), concerning the first set of NBS scenarios, the RG scenarios are relatively more cost-effective than the GR and PP scenarios. The most cost-effective scenario is RG1, with the CE value of around 2.9. In general, the scenarios with D_F (large-scale) lower than 1.6 are relatively more cost-effective (e.g. RG1, GR1, and PP1) because of their lower implementation level.

Regarding the second set of NBS scenarios (i.e. the four combined scenarios), the GR4+RG4 scenario is more cost-effective than the other combined scenarios. The PP4+RG4 scenario and PP4+RG4+GR4 scenario have the lowest CE ($\approx$ 0.38), which demonstrated that (i) increasing the implementation level of NBS in the catchment may not be the best solution considering both economic costs and hydrological performances; (ii) due to the hydrological performances of PP4+RG4 scenario are less effective comparing with the other combined scenarios, it is less cost-effective.

Regarding the fourth set of GR scenarios, the extensive GR scenario is much more cost-effective than the semi-intensive GR scenario, with the averaged CE around 0.88 (here, the CE is only computed for two different GR scenarios with the IS =10 %). Compared with the other NBS scenarios, the semi-intensive GR scenario is even less cost-effective than scenarios with combining two different NBS (i.e. PP4+GR4, RG4+GR4). Therefore, a high implementation level of

semi-intensive GRs in the catchment is not appropriate regarding the cost-effectiveness.

Concerning all NBS scenarios under the EV8 (Fig. 16d), the most cost-effective scenarios are the PP (upstream) and PP (downstream) scenarios, with the CE value of around 3.7. This result demonstrated that under the condition of the strong rainfall event characterised with some localised rainfall spikes, concentrating the single type of NBS in some specific locations in the catchment (e.g. the downstream in our studied catchment) is more cost-effective than heterogeneous implementing NBS over the whole catchment.

As shown in Fig. 17, a negative correlation was found between the cost-effectiveness of the NBS scenarios and their fractal dimensions. Namely, the cost-effective NBS scenarios are characterised by a relatively low D_F. It is noticed that the D_F of NBS scenarios is above 1.6, and the corresponding CE values are lower than 1.0 (the blue area in Fig. 17). The NBS scenarios with the D_F between 1.5 and 1.6 are more cost-effective than the D_F of NBS scenarios higher than 1.6, with the CE values ranging from 1.0 to 3.0. Unlike the aforementioned traditional indicators, the fractal dimension computed for each NBS scenario propagates the scales. Hence, the cost-effective NBS scenarios can be validated in this range of scales.

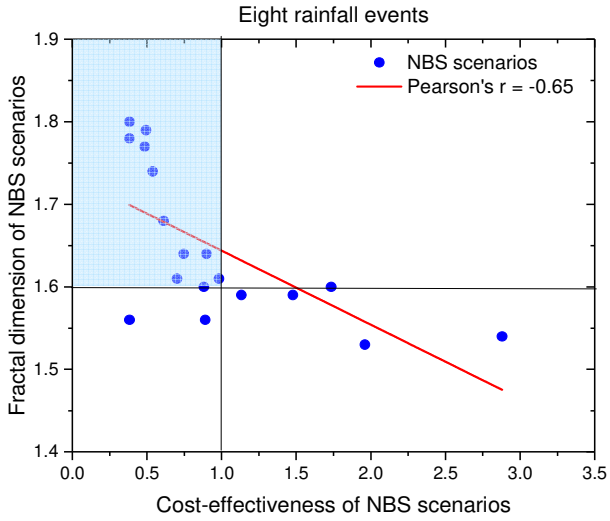

Fig. 17. Relationship between the fractal dimension of NBS scenarios and the cost-effectiveness of NBS scenarios for eight rainfall events.

Overall, these results are representative to transfer of the experiences to other catchments. Indeed, under the given economic investments, by quantifying the optimal D_F of NBS, the hydrological performance of NBS can be improved, and that of the life cycle costs can be reduced, so as to realise the spatial non-uniform distribution optimisation. Concerning the studied rainfall events, they are not extreme cases but somewhat representative. As the fractal dimension is a scale invariance indicator that conserves the performances for a wide range of scales, the results and the methodology shown in this study are quite general and can be scalable for application in other urban catchments with respect to the local conditions.

6. Conclusions

This paper focuses on evaluating the cost-effectiveness of nature-based solutions (NBS) scenarios by integrating technical and economic indicators under various rainfall conditions. We pointed out how the fractal dimension (D_F) can quantify the implementation levels and heterogeneous spatial distributions of NBS across scales, which is associated with the cost-effectiveness of NBS scenarios. The hydrological performances of NBS scenarios are firstly investigated with the help of the Multi-Hydro model under highly space-time variable rainfall events, and then quantified by hydrologic indicators. The economic costs of the NBS scenarios are based on assessing their life cycle costs. The principal findings are summarised as follows:

1) The hydrological performances of the NBS scenarios are indeed improved with the increase of their D_F (e.g. the PP4+RG4+GR4 scenario). However, due to some intersection effects of spatial variability in rainfall and NBS distributions, a non-linear relationship is found between the peak flow

reduction of NBS scenarios and the rainfall intensity. Under the strong rainfall event characterised by some localised rainfall spikes, implementing NBS downstream of the Guyancourt catchment is more effective than that of the upstream. The extensive GR scenario has the same hydrological performances as the semi-intensive GR scenario when the $IS < 50$ %. When the $IS = 50$ %, the hydrological performances of the semi-intensive GR scenario is significantly better than that of the extensive one under the rainfall events with a return period larger than one year.

2) The optimal/cost-effectiveness NBS scenarios have a relatively lower implementation level, characterised by D_F (large-scale) ranging from 1.5 to 1.6 (e.g. the most cost-effective scenario is RG1). The NBS scenarios are less cost-effective when their D_F is higher than 1.6 (e.g. combined scenarios). Regarding all NBS scenarios in the strongest event (EV8), the optimal NBS scenarios are PP upstream and PP downstream, which indicated that carefully concentrating a single type of NBS at specific locations can be more cost-effective than heterogeneous implementation NBS all over the catchment.

Overall, the obtained results can provide some effective guidelines for the decision-making process. In addition, the method proposed in this study can be scalable from one catchment to another in terms of local environmental conditions, which is helpful to find a universal solution for different catchments. Future work will be conducted to gain new insight into the scaling complexity of assessing the cost-effectiveness of NBS scenarios with the help of the Universal Multifractal framework across scales.

Acknowledgement

The first author greatly acknowledges the financial support by the China Scholarship Council (grant no. [2017]3109). The authors acknowledge the Chair "Hydrology for Resilient Cities" (endowed by VEOLIA), for partial financial support. The authors acknowledge Saint-Quentin-en-Yvelines agglomeration community for providing the data of Guyancourt catchment.

Declaration of Competing Interest

The authors report no declarations of interest.

Reference

Ahiablame, L., Shakya, R., 2016. Modeling flood reduction effects of low impact development at a watershed scale. J. Environ. Manage. 171, 81–91. doi.org/10.1016/j.jenvman.2016.01.036

Ahiablame, L.M., Engel, B.A., Chaubey, I., 2013. Effectiveness of low impact development practices in two urbanized watersheds: Retrofitting with rain barrel/cistern and porous pavement. J. Environ. Manage. 119, 151–161. doi.org/10.1016/j.jenvman.2013.01.019

Albert, C., Spangenberg, J., Schröter, B., 2017. Nature-based solutions: criteria. Nature 543, 315. doi.org/10.1038/543315a

Berretta, C., Poë, S., Stovin, V., 2014. Moisture content behaviour in extensive green roofs during dry periods: The influence of vegetation and substrate characteristics. J. Hydrol. 511, 374–386.

doi.org/10.1016/j.jhydrol.2014.01.036

Carter, T., Keeler, A., 2008. Life-cycle cost – benefit analysis of extensive vegetated roof systems. J. Environ. Manage. 87, 350–363. doi.org/10.1016/j.jenvman.2007.01.024Cipolla, S.S., Maglionico, M., Stojkov, I., 2016. A long-term hydrological modelling of an extensive green roof by means of SWMM. Ecol. Eng. 95, 876–887. doi.org/10.1016/j.ecoleng.2016.07.009

El Tabach, E., Tchiguirinskaia, I., Mahmood, O., and Schertzer, D., 2009. Multi-Hydro: a spatially distributed numerical model to assess and manage runoff processes in peri-urban watersheds. In Proceedings Final Conference of the COST Action C22 Urban Flood Management, Paris, 26 (no. 27.11).

European Commission, 2015. Towards an EU Research and Innovation policy agenda for Nature-Based Solutions & Re-Naturing Cities, Final Report of the Horizon 2020 Expert Group on "Nature-Based Solutions and Re-Naturing Cities", Luxembourg: Publications Office of the European Union, doi.org/10.2777/765301.

Eckart, K., Mcphee, Z., Bolisetti, T., 2017. Science of the Total Environment Performance and implementation of low impact development – A review. Sci. Total Environ. 607–608, 413–432. doi.org/10.1016/j.scitotenv.2017.06.254

Ercolani, G., Chiaradia, E.A., Gandolfi, C., Castelli, F., Masseroni, D., 2018. Evaluating performances of green roofs for stormwater runoff mitigation in a high flood risk urban catchment. J. Hydrol. 566, 830–845. doi.org/10.1016/j.jhydrol.2018.09.050

Fuller, S.K., and Petersen, S.R., 1996. Life-Cycle Costing Manual for the Federal Management Program. NIST handbook, 135, U.S. government printing office, Washington, D.C., United States.

Fry, T.J., Maxwell, R.M., 2017. Evaluation of distributed BMPs in an urban watershed—High resolution modeling for stormwater management. Hydrol. Process. 31, 2700–2712. doi.org/10.1002/hyp.11177

Giangola-murzyn, A., 2013. Hydrological modelling and parameterisation of the city, resilience to floods (Modélisation et paramétrisation hydrologique de la ville, résilience aux inondations).

Doctoral dissertation, Université Paris-Est, France.

Grebel, J.E., Mohanty, S.K., Torkelson, A.A., Boehm, A.B., Higgins, C.P., Maxwell, R.M., Nelson, K.L., Sedlak, D.L., 2013. Engineered infiltration systems for urban stormwater reclamation. Environ. Eng. Sci. 30, 437–454. doi.org/10.1089/ees.2012.0312

Guo, X., Du, P., Zhao, D., Li, M., 2019. Modelling low impact development in watersheds using the storm water management model. Urban Water J. 16, 146–155. doi.org/10.1080/1573062X.2019.1637440

Gutierrez-Lopez, A., Hernandez, S.B.J., Sandoval, C.E., 2019. Physical parameterization of IDF curves based on short-duration storms. Water (Switzerland) 11, 1–14. doi.org/10.3390/w11091813

Her, Y., Jeong, J., Arnold, J., Gosselink, L., Glick, R., Jaber, F., 2017. A new framework for modeling decentralized low impact developments using Soil and Water Assessment Tool. Environ. Model. Softw. 96, 305–322. doi.org/10.1016/j.envsoft.2017.06.005

Helmi, N.R., Verbeiren, B., Mijic, A., van Griensven, A., Bauwens, W., 2019. Developing a modeling tool to allocate Low Impact Development practices in a cost-optimized method. J. Hydrol. 573, 98–108. doi.org/10.1016/j.jhydrol.2019.03.017

Hua, P., Yang, W., Qi, X., Jiang, S., Xie, J., Gu, X., Li, H., Zhang, J., Krebs, P., 2020. Evaluating the effect of urban flooding reduction strategies in response to design rainfall and low impact development. J. Clean. Prod. 242, 118515. doi.org/10.1016/j.jclepro.2019.118515

Ichiba, A., 2016: X-Band Radar Data and Predictive Management in Urban Hydrology. Doctoral dissertation, Université Paris-Est, France.

Ichiba, A., Gires, A., Tchiguirinskaia, I., Schertzer, D., Bompard, P., Veldhuis, M.C. Ten, 2018. Scale effect challenges in urban hydrology highlighted with a distributed hydrological model. Hydrol. Earth Syst. Sci. 22, 331–350. doi.org/10.5194/hess-22-331-2018

Lovejoy, S., Schertzer, D., Tsonis, A.A., 1987. Functional Box-Counting and Multiple Elliptical Dimensions in Rain. Science (80). 235, 1036–1038. doi.org/10.1126/science.235.4792.1036

Leimgruber, J., Krebs, G., Camhy, D., Muschalla, D., 2019. Model-based selection of cost-effective low impact development strategies to control water balance. Sustain. 11. doi.org/10.3390/su11082440

Li, Y., Huang, J.J., Hu, M., Yang, H., Tanaka, K., 2020. Design of low impact development in the urban context considering hydrological performance and life-cycle cost. J. Flood Risk Manag. 13, 1–15. doi.org/10.1111/jfr3.12625

Liao, Z.L., He, Y., Huang, F., Wang, S., Li, H.Z., 2013. Analysis on LID for highly urbanized areas' waterlogging control: Demonstrated on the example of Caohejing in Shanghai. Water Sci. Technol. 68, 2559–2567. doi.org/10.2166/wst.2013.523

Liu, Y., Ahiablame, L.M., Bralts, V.F., Engel, B.A., 2015. Enhancing a rainfall-runoff model to assess the impacts of BMPs and LID practices on storm runoff. J. Environ. Manage. 147, 12–23. doi.org/10.1016/j.jenvman.2014.09.005

Luan, B., Yin, R., Xu, P., Wang, X., Yang, X., Zhang, L., Tang, X., 2019. Evaluating Green Stormwater Infrastructure strategies ef fi ciencies in a rapidly urbanizing catchment using SWMM-based TOPSIS. J. Clean. Prod. 223, 680–691. doi.org/10.1016/j.jclepro.2019.03.028

Mandelbrot, B. B., 1983. The fractal geometry of nature, W.H. Freeman and Company, New York, United States, 468.

Montalto, F., Behr, C., Alfredo, K., Wolf, M., Arye, M., Walsh, M., 2007. Rapid assessment of the cost-effectiveness of low impact development for CSO control. Landsc. Urban Plan. 82, 117–131. doi.org/10.1016/j.landurbplan.2007.02.004

Moriasi, D.N., Arnold, J.G., Liew, M.W. Van, Bingner, R.L., Harmel, R.D., Veith, T.L., 2007. Model evaluation guidelines for systematic quantification of accuracy in watershed simulations. Trans. ASABE 50, 885–900.

Nash, J. E., and Sutcliffe, J. V., 1970. River flow forecasting through conceptual models part I – A discussion of principles, J. Hydrol., 10, 282–290, doi.org/10.1016/0022-1694(70)90255-6.

Palla, A., Gnecco, I., 2015. Hydrologic modeling of Low Impact Development systems at the urban

catchment scale. J. Hydrol. 528, 361–368. https://doi.org/10.1016/j.jhydrol.2015.06.050

Praticò, F.G., Amodeo, L., Lamari, D., Lanciano, C., Placido, V., Praticò, M., Scattareggia, T., 2015. Pavement life cycle cost analysis for city logistics. WIT Trans. Built Environ. 146, 337–348. doi.org/10.2495/UT150271

Qiu, Y., Paz, I., Chen, F., Versini, P.-A., Schertzer, D., Tchiguirinskaia, I., 2021. Space variability impacts on hydrological responses of nature-based solutions and the resulting uncertainty: a case study of Guyancourt (France). Hydrol. Earth Syst. Sci. 25, 3137–3162. https://doi.org/10.5194/hess-25-3137-2021

Rossman, L. A., 2010: Storm water management model user's manual, version 5.0, 276, Cincinnati: National Risk Management Research Laboratory, Office of Research and Development, US Environmental Protection Agency, United States.

Richard, J., Giangola-Murzyn, A., Tchiguirinskaia, I., and Schertzer, D., 2013. MH-ASSIMTOOL: An assimilation tool dedicated to a fully distributed model. Poster presented at International Conference on Flood Resilience, 5–7 September 2013, Exeter, United Kingdom.

Schertzer, D., Lovejoy, S., 1987. Physical modeling and analysis of rain and clouds by anisotropic scaling mutiplicative processes. J. Geophys. Res. 92, 9693–9714. doi.org/10.1029/JD092iD08p09693

Scholz, M., Grabowiecki, P., 2007. Review of permeable pavement systems. Build. Environ. 42, 3830–3836. doi.org/10.1016/j.buildenv.2006.11.016

Spatari, S., Yu, Z., Montalto, F.A., 2011. Life cycle implications of urban green infrastructure. Environ. Pollut. 159, 2174–2179. doi.org/10.1016/j.envpol.2011.01.015

Stanić, F., Cui, Y.J., Delage, P., De Laure, E., Versini, P.A., Schertzer, D., Tchiguirinskaia, I., 2019. A device for the simultaneous determination of the water retention properties and the hydraulic conductivity function of an unsaturated coarse material; application to a green-roof volcanic substrate. Geotech. Test. J. 43. doi.org/10.1520/GTJ20170443

Velleux, M.L., England, J.F., Julien, P.Y., 2008. TREX: spatially distributed model to assess

watershed contaminant transport and fate. Sci. Total Environ. 404, 113–128. doi.org/10.1016/j.scitotenv.2008.05.053

Versini, P.A., Gires, A., Tchiguirinskaia, I., Schertzer, D., 2020. Fractal analysis of green roof spatial implementation in European cities. Urban For. Urban Green. 49, 126629. doi.org/10.1016/j.ufug.2020.126629

Versini, P.A., Gires, A., Tchinguirinskaia, I., Schertzer, D., 2016. Toward an operational tool to simulate green roof hydrological impact at the basin scale: A new version of the distributed rainfall-runoff model Multi-Hydro. Water Sci. Technol. 74, 1845–1854. doi.org/10.2166/wst.2016.310

Versini, P.A., Ramier, D., Berthier, E., de Gouvello, B., 2015. Assessment of the hydrological impacts of green roof: From building scale to basin scale. J. Hydrol. 524, 562–575. doi.org/10.1016/j.jhydrol.2015.03.020